









To my parents,  
for their love and guidance.



FLUORESCENCE SPECTRA AND AB INITIO  
THEORETICAL STUDIES OF HCOOH

by

Francesca Ioannoni, B.Sc.

A Thesis  
Submitted to  
the Department of Chemistry  
Brock University

In partial fulfillment  
of the requirements for the degree  
Master of Science

Brock University  
St. Catharines, Ontario  
July 1989

© F. Ioannoni, 1989





## ABSTRACT

A fluorescence excitation spectrum of formic acid monomer ( $\text{HCOOH}$ ), has been recorded in the 278-246 nm region and has been attributed to an  $n \rightarrow \pi^*$  electron promotion in the anti conformer. The  $S_1 \leftarrow S_0$  electronic origins of the  $\text{HCOOH}/\text{HCOOD}/\text{DCOOH}/\text{DCOOD}$  isotopomers were assigned to weak bands observed at 37431.5/37461.5/37445.5/37479.3  $\text{cm}^{-1}$ . From a band contour analysis of the  $0_0^0$  band of  $\text{HCOOH}$ , the rotational constants for the excited state were estimated:  $A'=1.8619$ ,  $B'=0.4073$ , and  $C'=0.3730$   $\text{cm}^{-1}$ . Four vibrational modes,  $\nu_3(\text{C=O})$ ,  $\nu_7(\text{O-C=O})$ ,  $\nu_8(\text{C-H}_{\text{ald}})$  and  $\nu_9(\text{O-H}_{\text{hyd}})$  were observed in the spectrum. The activity of the antisymmetric aldehyde wagging and hydroxyl torsional modes in forming progressions is central to the analysis, leading to the conclusion that the two hydrogens are distorted from the molecular plane,  $\text{O-C=O}$ , in the upper  $S_1$  state.

Ab initio calculations were performed at the 6-31G\* SCF level using the Gaussian 86 system of programs to aid in the vibrational assignments. The computations show that the potential surface which describes the low frequency OH torsion (twisting motion) and the CH wagging (molecular inversion) motions is complex in the  $S_1$  excited electronic state. The OH and CH bonds were calculated to be twisted with respect to the  $\text{O-C=O}$  molecular frame by 63.66 and 45.76 degrees, respectively. The calculations predicted the existence of the



second (syn) rotamer which is  $338\text{ cm}^{-1}$  above the equilibrium configuration with OH and CH angles displaced from the plane by 47.91 and 41.32 degrees.



## ACKNOWLEDGEMENTS

There are a number of people who have played an important role in the completion of this thesis. Their guidance, knowledge, patience, friendship and support have been greatly appreciated.

I wish to thank Dr. D. C. Moule for suggesting the problem and for guiding me through the research. I would also like to thank Dr. D. J. Clouthier at the University of Kentucky for his assistance with the experimental aspects of this study and for giving me the opportunity to work in his lab. Furthermore, I would like to express my gratitude to Dr. J. D. Goddard at Guelph University and R. B. Ogawa for their assistance in the ab initio calculations. A special thank you to Mr. D. J. Adams, of the computing Centre for his cooperation with the computational aspect of the thesis.

One group of people that I would like to acknowledge are the professors from the Chemistry, Physics and Math departments who have all contributed to my education. Their guidance throughout the years has allowed me to develop as a chemist and an individual. I greatly appreciate their dedication, patience and support. I especially want to thank two people, Dr. S. M. Rothstein and Dr. E. A. Cherniak for being not only advisors in the field of physical chemistry, but friends.



The financial assistance I received from the Ontario Graduate Scholarship program is greatly appreciated. This work was also supported by the Natural Sciences and Engineering Research Council of Canada.

I would like to thank the members of staff, both at the University of Kentucky and at Brock University, for their help and encouragement. Also, to my friends both at Kentucky and Brock, thank you for your interest and moral support.

A special thank you to the following people who helped me with the finishing touches on the thesis: Mr. F. Divino, Caroline Starrs, Jeff Martin, my sister Pam and brother Domenic. Lastly, to the most important group of people, my family, no words can express my thanks for all your encouragement, understanding, support and love.





## TABLE OF CONTENTS

	PAGE
CHAPTER 1	INTRODUCTION.....1
CHAPTER 2	AB INITIO CONCEPTS
2.1	Ab Initio Methods.....15
2.2	Molecular Structure Methods.....22
2.3	Molecular Vibrations.....29
CHAPTER 3	PRINCIPLES OF ELECTRONIC SPECTROSCOPY
3.1	Electronic Transitions.....31
3.2	Vibrational Structure.....37
3.3	Rotational Structure.....42
CHAPTER 4	EXPERIMENTAL
4.1	Fluorescence Spectroscopy.....46
4.2	Photoacoustic Spectroscopy.....52
4.3	Supersonic Jet Spectroscopy.....54
CHAPTER 5	RESULTS AND DISCUSSIONS
5.1	Fluorescence Excitation Spectra.....57
5.2	Theoretical Calculations.....74
CHAPTER 6	REMARKS AND CONCLUSIONS.....92
REFERENCES	100



# LIST OF TABLES

	Page
TABLE 1: STRUCTURES OF FORMIC ACID CONFORMERS	5
TABLE 2: MOLECULAR PARAMETERS FOR FORMIC ACID	6
TABLE 3: THE $C_s$ POINT GROUP CHARACTER TABLE	8
TABLE 4: VIBRATIONAL FREQUENCIES FOR FORMIC ACID MONOMER	9
TABLE 5: Z-MATRICES FOR THE GROUND AND EXCITED STATES OF FORMIC ACID	24
TABLE 6: OBSERVED BAND HEADS IN THE EXCITATION SPECTRA OF FORMIC ACID: HCOOH, HCOOD	64
TABLE 7: OBSERVED BAND HEADS IN THE EXCITATION SPECTRA OF FORMIC ACID: DCOOH, DCOOD	65
TABLE 8: OBSERVED $P_{Q_k}$ SUBBAND HEADS IN THE ROTATIONAL SPECTRUM OF THE $0_0^0$ BAND IN FORMIC ACID	67
TABLE 9: MOLECULAR STRUCTURE OF FORMIC ACID IN THE $S_0$ GROUND AND $T_1$ ELECTRONIC STATES	75
TABLE 10: TOTAL ENERGY OF FORMIC ACID IN THE $S_0$ AND $T_1$ ELECTRONIC STATES	76
TABLE 11: VIBRATIONAL FREQUENCIES OF FORMIC ACID IN THE $S_0$ AND $T_1$ ELECTRONIC STATES	78
TABLE 12: DISPLACEMENTS FOR THE NORMAL VIBRATIONS OF ANTI FORMIC ACID IN THE $T_1$ STATE	84
TABLE 13: DISPLACEMENTS FOR THE NORMAL VIBRATIONS OF SYN FORMIC ACID IN THE $T_1$ STATE	85
TABLE 14: CALCULATED MOLECULAR STRUCTURE OF FORMIC ACID IN THE $S_0$ GROUND AND $S_1$ ELECTRONIC STATES	86
TABLE 15: CALCULATED TOTAL ENERGY OF FORMIC ACID IN THE $S_0$ AND $S_1$ ELECTRONIC STATES	87
TABLE 16: CALCULATED EQUILIBRIUM ROTATIONAL CONSTANTS AND DIPOLE MOMENTS FOR THE $S_0$ AND $S_1$ STATES	90



## LIST OF FIGURES

	Page
Figure 1: The molecular structures of HCOOH including the symmetry and principal axes	3
Figure 2: Localized MO's and the Electronic Transitions for the carbonyl group of Formic Acid	10
Figure 3: Logical Structure of a typical <u>ab initio</u> molecular orbital program	16
Figure 4: Closed-shell singlet and open-shell triplet orbital configurations of HCOOH	20
Figure 5: Sequence of program execution for a molecular geometry optimization	23
Figure 6: Possible vibronic transitions in the $\tilde{A}^1A'' \leftarrow \tilde{X}^1A'$ electronic transition of HCOOH	36
Figure 7: Correlation diagram for the energy levels of rigidly planar and flexible nonplanar structures	41
Figure 8: Schematic diagram of the instrumentation for Laser-induced fluorescence	47
Figure 9: Diagram of the optical light path through the fluorescence excitation cell	49
Figure 10: Photograph of the experimental set-up in the laboratory for fluorescence spectroscopy	50
Figure 11: Schematics of the Photoacoustic cell	53
Figure 12: Description of the cell compartment set-up used for supersonic jet spectroscopy	55
Figure 13: Laser induced fluorescence excitation spectrum of formic acid, HCOOH from 37300 - 40500 $\text{cm}^{-1}$	58



	Page
Figure 14: Laser induced fluorescence excitation spectrum of formic acid, HCOOD from 37300 - 40500 $\text{cm}^{-1}$	59
Figure 15: Laser induced fluorescence excitation spectrum of formic acid, DCOOH from 37300 - 40500 $\text{cm}^{-1}$	60
Figure 16: Laser induced fluorescence excitation spectrum of formic acid, DCOOD from 37300 - 40500 $\text{cm}^{-1}$	61
Figure 17: Laser induced fluorescence excitation spectrum of formic acid, HCOOH from 35900 - 37500 $\text{cm}^{-1}$	63
Figure 18: The rotational spectrum of the $0_0^0$ band of HCOOH recorded at 1 Torr, 0.05 $\text{cm}^{-1}$ resolution and 60°C	66
Figure 19: Plots of the residuals versus literature values for the U/Ar lines identified for the calibration of the experimental spectra	68
Figure 20: Observed $0_0^0$ band and the computed A-type, B-type and C-type bands	73
Figure 21: Description of the vibrational frequencies of the normal mode coordinates for Anti and Syn HCOOH, respectively in the $S_0$ state	79
Figure 22: Newman projection diagrams illustrating the Molecular structure of formic acid in the ground $S_0$ and $T_1$ excited electronic states	81
Figure 23: Photographs of the calculated ground state and singlet excited state geometries of Anti and Syn formic acid, respectively	88
Figure 24: Description of the antisymmetric $p_z$ molecular orbitals of anti formic acid	97





## CHAPTER 1

### INTRODUCTION

Formic acid is the parent member of the carboxylic acid series. This stable molecule can be isolated from the distillation of ants, or industrially prepared by the reaction of carbon monoxide with sodium hydroxide at 200<sup>0</sup>C, followed by acidification with HCl and distillation.<sup>1</sup> In ants, formic acid serves the dual purpose of defence and communication. Moreover, formic acid plays a part in the swelling and irritation associated with ant bites and bee stings. On the atmospheric level, scientists are concerned about formic acid as it provides most of the acidity for the acid rain that falls on remote areas.<sup>2</sup> Hence, the production of formic acid is significant for industrial uses and environmental interests.

There is also considerable interest in the spectroscopy of formic acid. Interstellar HCOOH has been detected from the direction of the galactic centre radio source Sagittarius B2.<sup>3</sup> Besides the value of formic acid to photophysics, the spectroscopy of this carbonyl molecule is important for the photochemical studies of the photodissociation products, OH and CHO. Therefore, a clear understanding of the structure and dynamics of this simple molecular system in both the ground and excited states is essential. Although the ground state is well characterized by microwave, infrared, electron



diffraction studies and ab initio calculations; the excited states of formic acid are not well known. The present laser spectroscopic and quantum chemical investigations have been undertaken to provide information about the behaviour of formic acid in its first excited electronic state. With this exploration, the structure and dynamics of formic acid can be extended, and should lead to further avenues of research and greater comprehension.

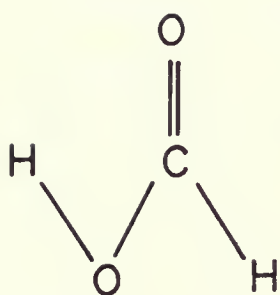
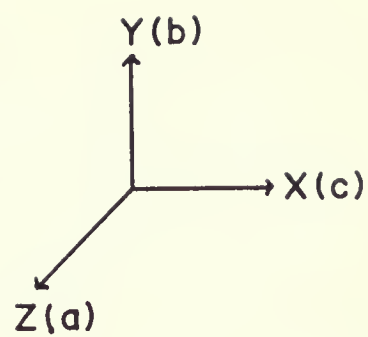
In the vapour phase, formic acid can exhibit rotational isomerism as a consequence of the restricted internal rotation about the C-O bond. A representation of these two planar rotameric forms is depicted in Figure 1. Early infrared<sup>4,5</sup> and electron diffraction<sup>6</sup> work indicated that the anti(trans) species was the predominant form. These results were later confirmed by further infrared<sup>7,8</sup> and electron diffraction<sup>9-11</sup> studies. More recently, refined molecular structures have been determined for anti HCOOH by microwave<sup>12-15</sup> and electron diffraction<sup>16</sup> studies.

The experimental identification of the syn(cis) rotamer; however, was not conclusive.<sup>17-19</sup> There have been several tentative assignments of a few infrared absorption bands to syn HCOOH, but the positive identification of the syn rotamer was not until 1976 when the spectrum of syn formic acid was observed directly. From a careful analysis of the weak lines in the microwave spectrum, Hocking<sup>20</sup> showed that the syn

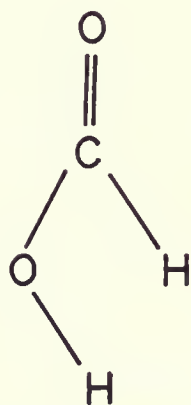


Figure 1  
The molecular structures of HCOOH including the  
symmetry and the principal axes





*anti* HCOOH



*syn* HCOOH





conformer was present in the vapour phase to the extent of 0.13% and that the energy difference between the two forms was  $1365\text{ cm}^{-1}$  ( $3900\text{ cal/mol}$ ), with the anti rotamer being at lower energy. Furthermore, the barrier to internal rotation for anti $\rightarrow$ syn was estimated to be  $4840\text{ cm}^{-1}$  ( $13.8\text{ kcal/mol}$ ). The complete substitution structure of syn HCOOH has also been determined.<sup>21</sup> The microwave structures for both the anti and syn geometrical isomers are collected in Table 1. In addition, equilibrium ab initio structures calculated at the self-consistent-field (6-31G\*) level have recently been determined<sup>22</sup> for the conformers and are reported. These theoretical calculations place the syn planar rotamer about  $2140\text{ cm}^{-1}$  higher in energy than the anti planar configuration. In Table 2 the molecular parameters determined from microwave studies for formic acid are listed.

Besides exhibiting rotational isomerism, formic acid is known to dimerize. Thermochemical studies<sup>23</sup> place the enthalpy of dimer formation at  $5180\text{ cm}^{-1}$  ( $14.8\text{ kcal/mol}$ ). Ab initio SCF calculations<sup>24</sup> gave a value of  $4370\text{ cm}^{-1}$  ( $12.5\text{ kcal/mol}$ ). The experimental determination of the equilibrium dimer structure is based on electron diffraction measurements.<sup>16,25</sup> An optimised equilibrium geometry of the formic acid dimer,  $(\text{HCOOH})_2$ , at various levels of ab initio SCF theory has also been predicted.<sup>24</sup> The equilibrium between monomer and dimer has been investigated from various infrared



TABLE 1: STRUCTURES OF FORMIC ACID CONFORMERS<sup>a</sup>

	ANTI		SYN	
	Expt. <sup>b</sup>	Ab Initio <sup>c</sup> 6-31G*	Expt. <sup>d</sup>	Ab Initio 6-31G*
r(C=O)	1.202(5)	1.1819	1.195(3)	1.1755
r(C-H)	1.097(1)	1.0835	1.105(4)	1.0900
r(C-O)	1.343(1)	1.3229	1.352(3)	1.3285
r(O-H)	0.972(5)	0.9532	0.956(5)	0.9482
$\alpha$ (COH)	106.3(1)	108.72	109.7(4)	111.47
$\alpha$ (OCH)	124.1(1)	124.73	123.0(6)	123.16
$\alpha$ (OCO)	124.9(1)	124.88	122.4(4)	123.02

a) distances in Å, angles in degrees.

b) Ref. 14

c) Ref. 22

d) Ref. 21



TABLE 2: MOLECULAR PARAMETERS<sup>a</sup> FOR FORMIC ACID

	HCOOH	
	anti <sup>b</sup>	syn <sup>c</sup>
A	77.5122	86.4616
B	12.0551	11.6892
C	10.4161	10.2840
$\mu_a$	1.40	2.65
$\mu_b$	0.26	2.71
$\mu$	1.42	3.79

a) rotational constants in GHz; dipole moments in Debyes.

b) Ref. 15

c) Ref. 20



and Raman studies.<sup>26-32</sup> The equilibrium constant for dimer formation<sup>33,34</sup> is about  $150 \text{ atm}^{-1}$  at  $21^\circ\text{C}$ . This means that at 10 Torr the monomer/dimer ratio is 4:1 and at 35 Torr it is 2:1. In contrast, from photoelectron studies, the monomer/dimer ratio at room temperature in supersonic jets is estimated to be 1:3.<sup>35</sup>

Formic acid monomer belongs to the  $C_s$  point group. The character table given in Table 3 for this point group shows that there are only two symmetry operations possible; namely, reflection in the plane of the molecule and the identity operation. There are nine normal vibrational modes for the molecule: 7  $a'$ , symmetric and 2  $a''$ , antisymmetric species. The observed and calculated ab initio ground state vibrational frequencies of anti HCOOH are summarized in Table 4. The reported vibrational frequencies of  $\nu_3$  and  $\nu_7$  for the syn isomer are  $1744.7$  and  $1124.2 \text{ cm}^{-1}$ , respectively.<sup>19</sup>

The ground state electronic configuration of formic acid is:  $(1a')^2 \dots (8a')^2 (1a'')^2 (9a')^2 (2a'')^2 (10a')^2$ , where the first ten occupied orbitals represent the electrons in low energy molecular orbitals (MO's) followed by a  $\pi$  C=O MO and an n orbital for the carbonyl oxygen lone pair. As a consequence of electron promotion, both valence and Rydberg transitions are possible. A schematic representation of the localized MO's and electronic transitions for the carbonyl group are shown in Figure 2.





TABLE 3: THE  $C_S$  POINT GROUP CHARACTER TABLE

$C_S$	E	$\sigma_h$		
A'	1	1	$T_x, T_y; R_z$	$\alpha_{xx}, \alpha_{yy}, \alpha_{zz}, \alpha_{xy}$
A''	1	-1	$T_z; R_x, R_y$	$\alpha_{yz}, \alpha_{zx}$



TABLE 4: VIBRATIONAL FREQUENCIES<sup>a</sup> FOR FORMIC ACID MONOMER

Mode	Description	Expt. <sup>b</sup>	Ab Initio <sup>d</sup> (DZ + P)
$\nu_1$	(O-H)	3569	4116
$\nu_2$	(C-H)	2942	3293
$\nu_3$	(C=O)	1777	2015
$\nu_4$	(H-C-O)	1381	1536
$\nu_5$	(H-O-C)	1223 <sup>c</sup>	1426
$\nu_6$	(C-O)	1104	1268
$\nu_7$	(O-C=O)	625	690
$\nu_8$	(H-C oop)	1033	1183
$\nu_9$	(H-O oop)	642	693

a) in  $\text{cm}^{-1}$ . The theoretical prediction are harmonic frequencies while the experimental values are the observed (anharmonic) fundamentals.

b) Ref. 31

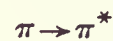
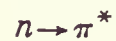
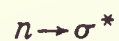
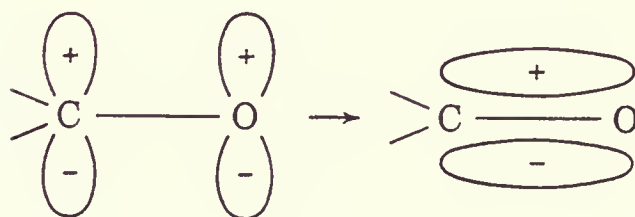
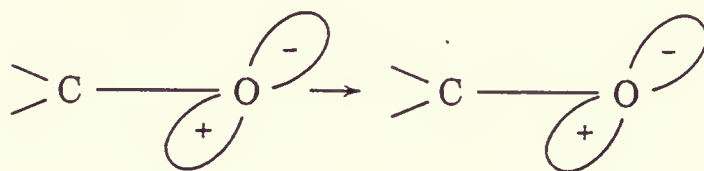
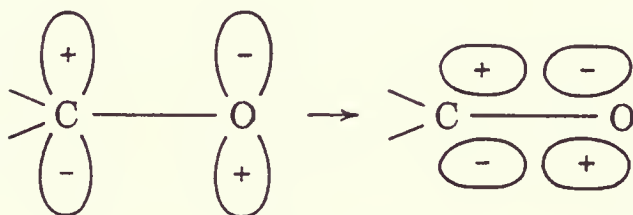
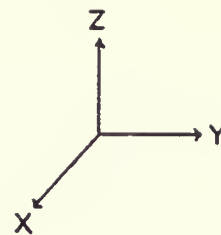
c) Ref. 19

d) Ref. 24



Figure 2  
Localized MO's and the Electronic Transitions  
for the carbonyl group of Formic Acid









The absorption spectrum of formic acid in the vacuum UV region was first observed in 1937.<sup>36</sup> The spectrum was mainly Rydberg in character. A further detailed investigation of formic acid in the 110-180 nm region at higher resolution<sup>37</sup> gave similar results. The most significant change in geometrical structure was an increase in the C=O bond length, and there was no evidence for non-planarity in these Rydberg states. Earlier studies<sup>38,39</sup> of the electronic spectra of formic acid vapour; however, identified the existence of a valence excitation,  $\pi \rightarrow \pi^*$ , in this region. Electron impact<sup>40,41</sup>, photoelectron spectra<sup>42</sup> and ab initio calculations<sup>43,44</sup> have also made contributions to the understanding of the optical absorption spectra of formic acid. Although there is considerable agreement in the results, the identity of a number of the Rydberg series and valence excitations is controversial.<sup>45,46</sup>

Further electronic absorption studies of HCOOH in the UV led to the detection of a diffuse band system<sup>47</sup> from 225 to 250 nm. More recently, at long absorption paths (60 m or greater) and at high resolution, weak but sharp bands displaying rotational fine structure in the near UV (250-270 nm) were observed by Ng and Bell.<sup>48</sup> Both the diffuse and sharp bands belong to the same vibrational system which is assigned to the  $n \rightarrow \pi^*$  electronic transition in the carbonyl group. Of particular interest is the latter study where a



detailed rotational analysis of a number of vibrational bands and the classification of many bands according to their band type were made. The spectra of the deuterated isotopomers were diffuse and the band structure was congested; therefore, the position of the origin band could not be located. Nevertheless, progressions of 1080 and 400  $\text{cm}^{-1}$  were found in the spectrum and assigned to the  $\nu_3$  (C=O) and  $\nu_7$  (O-C=O) modes, respectively. The activity of these modes is a consequence of changes in the C=O bond length and the OCO angle. From the analysis, though, the structure and dynamics of the formyl and hydroxyl hydrogens in this excited electronic state could not be determined.

Photochemical studies<sup>49-51</sup> from the late 1980's on formic acid provide useful insight on the structure of the hydroxyl group in the upper electronic state. The dynamics by which the OH group is ejected during the UV photodissociation of formic acid appear to be associated with the activity of the OH torsional mode,  $\nu_9$ . Since the anti and syn rotamers are planar in the lower  $S_0$  state, activity in the  $\nu_9$  mode implies that the OH group must be distorted from the plane in the upper electronic state. The formyl end of the molecule is also expected to be nonplanar. As the carbonyl moieties of HClCO/HFCO are isoelectronic with HCOOH, these molecules should possess similar properties. The  $S_1$  states of the HClCO/HFCO species are known to be pyramidal and the aldehyde



hydrogens adopt out-of-plane angles of 48.6/29.7 degrees, with barriers to inversion of 1609/2550  $\text{cm}^{-1}$ , respectively.<sup>52-54</sup>

In addition, since the electronegativities of the OH and Cl groups are similar, the potential function governing the molecular dynamics of the aldehyde hydrogen in the  $S_1$  state of formic acid should have a high central barrier. It follows that both the CH and the OH bond would be distorted from the O-C=O plane, which would give the  $S_1$  state an unusual structure.

In summary, formic acid has been extensively studied by the methods of optical spectroscopy and has been the subject of a number of theoretical studies. Only recently, however, has a detailed picture of the dynamics of this species begun to emerge. In the vapour phase, formic acid is known to exist in anti and syn planar conformations and formic acid dimerizes. These properties make this simple carboxylic acid spectroscopically very interesting.

The ground state properties of formic acid are reasonably well described; however, the role of geometrical isomerisation, dimerisation and the structural changes due to the excitation of formic acid are not clear. In the present work, the fluorescence excitation spectra of formic acid and its isotopomers have been recorded from 246-268 nm in order to study the structural properties of formic acid and to assign the vibrational frequencies of the  $S_1$  state. Ab initio



calculations describing the  $S_0$ ,  $T_1$ , and the  $S_1$  states were used as an aid in the assignment of the observed excitation spectra. Therefore, questions pertaining to the structure and dynamics of formic acid in the lowest excited electronic states were considered from the standpoint of laser excitation spectroscopy and high level ab initio molecular orbital calculations.





## CHAPTER 2

## AB INITIO MOLECULAR ORBITAL THEORY

(I) Ab Initio Methods

Ab initio chemical calculations can be used to predict the structures, energies, vibrational frequencies, and other properties of molecules. In particular, Gaussian 86<sup>55</sup> is a connected system of programs capable of performing ab initio molecular orbital (MO) calculations. It represents a further development of the Gaussian 70, 76, 80 and 82 systems already published. The logical structure of a typical program capable of performing molecular orbital calculations is presented in Figure 3. For the computations considered here, a VAX 11/780 computer was utilized. The input for the program includes: specification of the quantum mechanical method (energy calculation procedure), basis set, type of job, charge and multiplicity of the required electronic state and the molecular geometry.

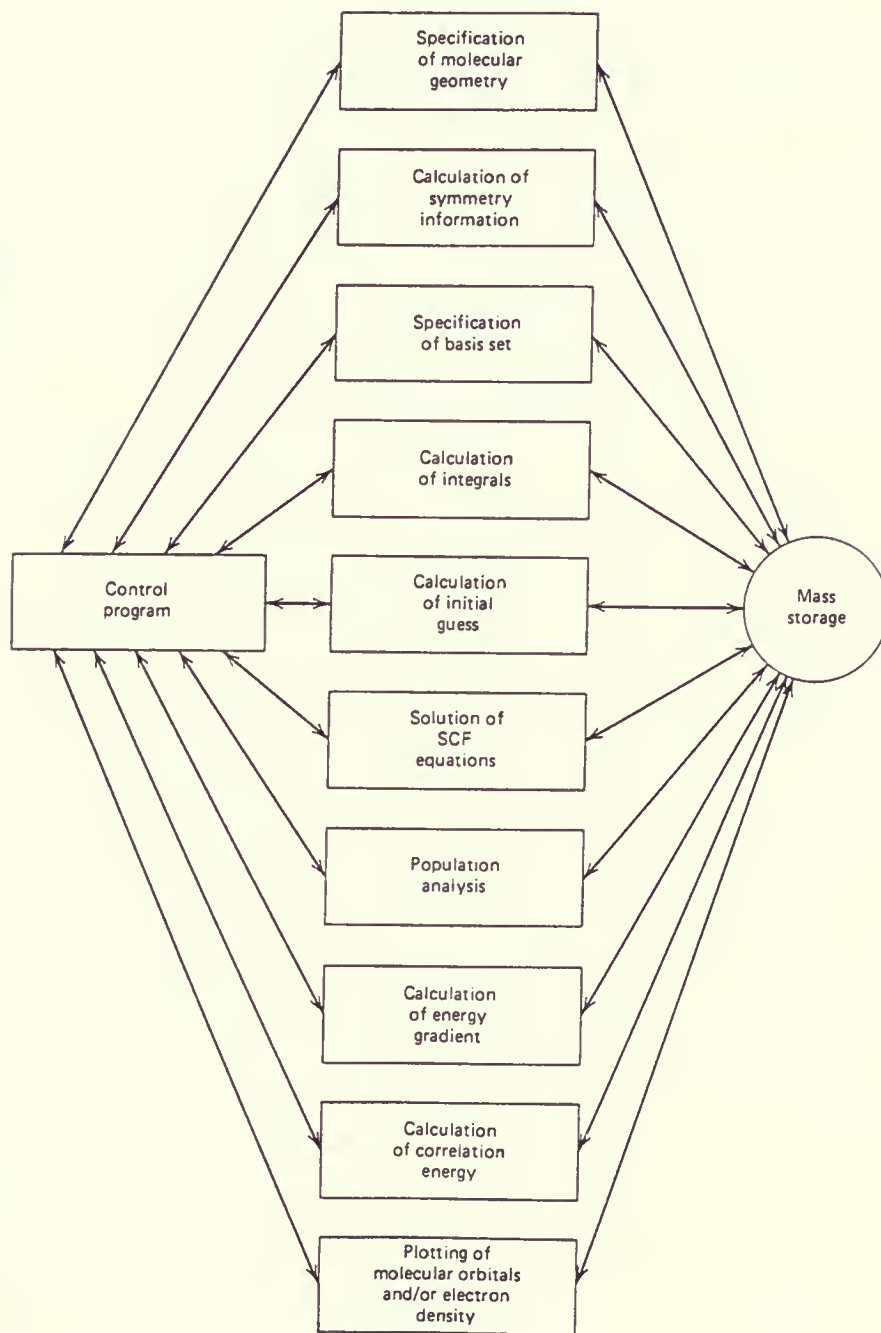
Ab initio theory makes use of the Born-Oppenheimer<sup>56</sup> approximation that the nuclei remain fixed on the time scale of electron movement. The Schrödinger equation<sup>57</sup> for the electrons becomes

$$\hat{H}\Psi = E\Psi \quad (2.1)$$



Figure 3  
Logical Structure of a typical ab initio  
molecular orbital program







where  $H$  is the electronic Hamiltonian corresponding to the motion of the electrons

$\Psi$  is the electronic wavefunction

and  $E$  is the electronic energy.

The main task of theoretical studies is to approximately solve the electronic Schrodinger equation.

In molecular orbital theory, electrons are assigned to molecular orbitals. These in turn are brought together to form a many-electron wavefunction. The molecular orbitals  $\psi_1, \psi_2, \dots$  are linear combinations of  $N$  known one-electron basis functions.

$$\psi_i = \sum_{\mu=1}^N c_{\mu i} \phi_{\mu} \quad (2.2)$$

These basis functions which are the atomic orbitals for the atoms in the molecule, constitute the basis set. In Gaussian 86, the MO calculations are performed within the linear combination of atomic orbitals (LCAO) framework. Given the basis set, the unknown coefficients,  $c_{\mu i}$ , are determined so that the total electronic energy, calculated from the many-electron wavefunction, is minimized and is as close to the energy corresponding to the exact solution of the Schrödinger equation.<sup>58</sup>

The variational method in quantum mechanics<sup>59</sup> can be mathematically described in the following manner for ab initio methods. If  $\Phi$  is an antisymmetric normalized function of the





electron coordinates, the expectation value of the energy corresponding to this function can be obtained from

$$\langle E \rangle = \int \Phi^* \hat{H} \Phi d\tau / \int \Phi^* \Phi d\tau \quad (2.3)$$

where integration is over the coordinates of all the electrons. If  $\Phi$  is the exact wavefunction,  $\Psi$ , the exact energy can be calculated; otherwise, the resulting energy will be as close to the exact value within the limitations imposed by (a) the single-determinant wavefunction, and (b) the particular basis set employed. In any event, the best wavefunction is found by minimizing  $\langle E \rangle$  with respect to the coefficients,  $c_{\mu_i}$ . This implies the variational condition

$$\frac{\delta E}{\delta c_{\mu_i}} = 0 \quad (\text{all } \mu, i) \quad (2.4)$$

Of particular significance to ab initio calculations is the self-consistent field (SCF) model. This method is also known as Hartree-Fock or single-determinant theory. At the SCF level, electrons are not allowed to avoid each other, but it is assumed that their instantaneous positions are independent of one another. The procedure involves an iterative process in which the orbitals are improved from cycle to cycle until the electronic energy reaches a constant value and the orbitals no longer change.<sup>60</sup> With Gaussian 86,



self-consistent field wavefunctions of the closed-shell Hartree-Fock (RHF), open-shell unrestricted Hartree-Fock (UHF), open-shell restricted Hartree-Fock (ROHF), and Generalized Valence Bond (GVB) forms can be determined.

In RHF<sup>61</sup> theory, one set of molecular orbitals is calculated where each orbital is doubly occupied or empty. In contrast, for the UHF<sup>62</sup> formalism, two sets of molecular orbitals are determined, one for each type of spin. These two sets of orbitals, referred to as alpha and beta, are similar, but not identical. Figure 4 depicts the differences between the RHF treatment for the closed-shell singlet ground state and the UHF treatment of the open-shell triplet excited state of formic acid. For the ROHF<sup>58</sup> procedure, the doubly occupied orbitals are restricted to being identical for alpha and beta spins.

The GVB<sup>63</sup> method, on the other hand, utilizes a multi-configuration wavefunction which uses non-orthogonal orbitals to describe a bonding pair of electrons. In this fashion, changes in bonding, antibonding and non-bonding of electrons are more adequately described than possible with HF wavefunctions.<sup>64</sup> Thus, at the SCF level, more than one configuration is considered allowing for the mixing of electronic states. In contrast to an HF wavefunction where a bond pair consists of one doubly occupied orbital, each valence electron in a GVB wavefunction is allowed to have a


















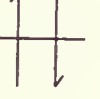

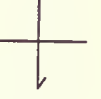






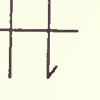





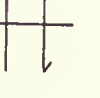




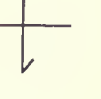



Figure 4  
Closed-shell singlet and open-shell triplet orbital  
configurations of HCOOH

RHF = restricted Hartree-Fock

UHF = unrestricted Hartree-Fock

$$\alpha = \uparrow \qquad \beta = \downarrow$$



3a''			
10a'			
2a''			
9a'			
1a''			
8a'			
7a'			
6a'			
5a'			
4a'			
3a'			
2a'			
1a'			

RHF

UHF





different orbital. The conventional closed-shell orbital description of a singlet electron pair is then replaced by a GVB pair consisting of two non-orthogonal orbitals coupled into a singlet.

$$\phi_a \phi_a \alpha \beta \rightarrow (\phi_{1a} \phi_{2a} + \phi_{2a} \phi_{1a}) \alpha \beta \quad (2.5)$$

Although each singlet electron pair is allowed to correlate; computationally, all orbitals other than the two within a given singlet pair are required to be orthogonal. Both the HF and GVB methods optimise the orbitals self-consistently.<sup>65</sup>

Post Hartree-Fock methods include configuration interaction<sup>58</sup> (CI) based on the single determinant wavefunctions and Moller-Plesset perturbation theory.<sup>66</sup> The Gaussian 86 package can compute double or single and double excitations for CI and determine contributions to fourth order (MP2, MP3, MP4) perturbation theory. These procedures account for the correlation of electron motion and are corrections to the SCF energy.

For the computations considered in this study, the energy procedures used involved RHF and GVB-Perfect-Pairing techniques for the closed-shell ground state; UHF methods for the open-shell triplet excited state; and, GVB (Open Shell Singlet) for the singlet excited state. Attempts at describing the first excited singlet state with the ROHF



method were unsuccessful. Post Hartree-Fock methods were not considered in this study as these calculations are computer time prohibitive and resource intensive.

## (II) Molecular Structure Optimization

A typical flow chart for an ab initio geometry optimization is given in Figure 5. The description of the molecular geometry is specified in the form of a Z-matrix with defined bond lengths, bond angles and dihedral angles. The Z-matrix is a geometrical device used to define the positions and types of atoms in the system. It doesn't tell the program where to put bonds or to represent a given electronic state.<sup>60</sup> The Z-matrices for the ground and excited states of formic acid are given in Table 5. To understand the input formulation, the ground state Z-matrix for anti-HCOOH will be discussed. The first atom, in this case, C, is always placed at the origin of the coordinate system. The second atom, O, is defined by the distance  $r_{\text{cod}}$  from atom 1. The third atom, the aldehyde hydrogen, is bound to atom 1 at a distance of  $r_{\text{ch}}$ , making an angle with atom 2 of  $\text{och}$ . The fourth atom, O, is defined exactly as the third, except an extra parameter is needed to specify its position uniquely. This atom is bound to the carbon, number 1, at a distance of  $r_{\text{cos}}$ , making an angle with the carbonyl oxygen, number 2, of  $\text{oco}$ , and a dihedral angle with the hydrogen atoms number 3 of  $180^\circ$ . In



Figure 5  
Sequence of program execution for a molecular  
geometry optimization



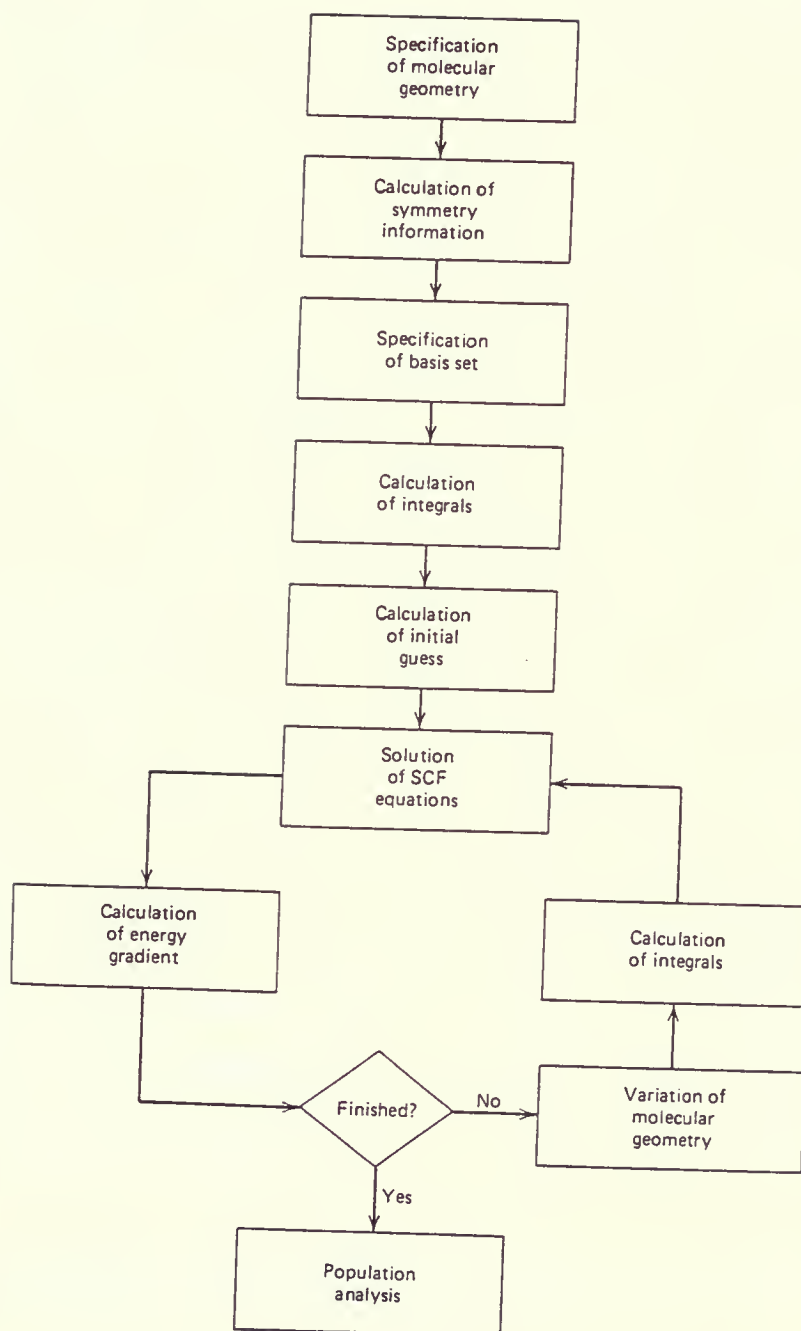






TABLE 5: Z-MATRICES FOR THE GROUND AND EXCITED STATES OF FORMIC ACID<sup>a</sup>

## (1) Planar Ground State

anti HCOOH

C

O 1 rcod

H 1 rch 2 och

O 1 rcos 2 oco 3 180.0 0

H 4 roh 1 coh 2 0.0<sup>b</sup> 0

## (2) Excited States

Nonplanar

Planar

C

O 1 rcod

X 1 1.0 2 90.0

H 1 rch 3 xch 2 alpha1 0

O 1 rcos 3 90.0 2 alpha2 0

H 5 roh 1 coh 2 theta 0

C

O 1 rcod

X 1 1.0 2 90.0

H 1 rch 3 90.0 2 alpha1 0

O 1 rcos 3 90.0 2 alpha2 0

H 5 roh 1 coh 2 0.0<sup>c</sup> 0

- a) for simplicity, the variable values have been excluded from the Z-matrix input.
- b) this value becomes 180.0 for the syn HCOOH calculation and for the determination of the transition state, it is replaced by a variable.
- c) this value becomes 180.0 for the syn HCOOH calculation.



general, the dihedral angle is obtained by imagining a Newman projection along the bond between the atom to which the current atom is bonded and that with reference to which the angle is defined.<sup>60</sup> The final atom, number 5, is defined in an identical manner.

For the excited state calculations, the Z-matrix description geometry is similar to that seen for the ground state; however, a dummy atom, X, has been included to facilitate interpretation of the results of the calculation. The role of the dummy atom is to define a specific set of geometrical parameters suitable for use in the structure optimization of formic acid. The dummy atom is merely a point in space used for geometry definition, and the cartesian coordinates generated for dummy atoms are not utilized in the quantum mechanical calculations, leaving the real molecule.<sup>58</sup>

The information from the Z-matrix is used to calculate the Cartesian (x,y,z) coordinates of the atoms. Knowing the geometry, charge (0,1,2,...), atomic numbers, and multiplicity (singlet, doublet or triplet) the total number of electrons, symmetry and orbital occupancies are determined. The atomic orbitals are then assigned to each nucleus. For the calculations, an internally stored standard set of coefficients and exponents were used to define the orbitals. The basis set utilized for the HCOOH calculations was 6-31G\*. This is known as a split valence basis set with polarization,



where the orbitals are described by Gaussian functions.<sup>58</sup> A split valence basis set is one where hydrogen and helium are represented by two s-type functions, and the first and second row atoms are given by two complete sets of valence s and p functions. Each inner or core atomic orbital is expressed in terms of six Gaussians. The valence-shell orbitals are described by three contracted and one diffuse basis function. Lastly, charge polarization, designated by \*, has been included to allow for the possibility of non-uniform displacement of charge away from the atomic centres. Six d-type Gaussian primitives are added in the basis set for every non-hydrogen atom in the system.

Ab initio programs next calculate the various one- and two-electron integrals required in the calculations. An initial guess involving a trial set of molecular orbitals is then made. For the calculations considered, the form of the initial guess was that obtained from an INDO<sup>67</sup> semi-empirical calculation. The initial guess is used as the starting point for the iterative SCF calculation. The solution to the SCF equations is improved cycle by cycle until the electronic energy is at a minimum. Using the determined wavefunction the energy gradient, first derivatives of the energy with respect to displacements in the nuclear coordinates, is evaluated. If the gradient is below some preset limit, then the specified geometry represents a stationary point on the potential energy



surface and the optimization is terminated. On the other hand, if the calculated gradient is larger than the allowed tolerance, the original geometry is varied followed by a new calculation of integrals, SCF energy and the energy gradient. The number of passes depends on several factors: the number of independent geometrical variables, the convergence criteria and the choice of the starting structure. Generally, for a system with  $n$  variables, between  $n$  and  $2n$  cycles are needed to ensure that the bond lengths and angles have converged to within  $0.0001 \text{ \AA}$  and  $0.1^\circ$ , respectively.<sup>58</sup> When the optimization is complete, the program moves on to a population analysis of the optimised species.

Geometry optimization programs are designed to find stationary points on a potential energy surface. Of particular importance to this work are minima, for which all normal vibrations are positive; saddle points or transition states, which have one negative eigenvalue in the force-constant matrix; and, maxima, which are described by two negative eigenvalues.<sup>59</sup> These definable points on the potential surface of the singlet ground state and the triplet excited state were determined using the RHF and UHF approximations, respectively. These procedures were directly used and only required adjusting the multiplicity to 0 or 3 as needed for the calculation.





The minima for both the singlet ground and excited states were probed successfully using the GVB technique. To look at the singlet excited state, a number of options available in Gaussian 86 were used to produce an electronic configuration having orbitals in the correct order, localized and of the desired symmetry. For the closed-shell ground state of anti and syn formic acid, calculations were performed with virtual orbitals 13 and 14 being swapped and one GVB-Perfect-Pair being formed with orbitals 10 and 11, which describe the carbonyl end of the molecule. For the singlet excited state, the GVB(OSS) option was utilized where the highest occupied and lowest virtual orbital from the guess are coupled as an open-shell singlet. To ensure that the  $n$  orbital was being coupled with  $\pi^*$ , orbital 13, it was necessary to interchange orbital 11 with 12 for the anti species; and, similarly, orbital 10 was swapped with 12 for the syn species. In this way, the optimised geometries for the desired singlet electronic states could be obtained. For the ROHF calculation, an alter option is essential. However, it was discovered that whether the  $\alpha$  or  $\beta$  spin of orbital 12 was swapped with 13, the desired excited singlet state configuration could not be achieved. Due to this difficulty, optimised geometries for the singlet excited state could not be determined from this HF approximation.



## (III) Molecular Vibrations

The optimised geometry is used as the input for a vibrational frequency calculation. In Gaussian 86, analytical second derivatives of the RHF and UHF energies can be computed and used to predict vibrational frequencies. These can also be evaluated by numerically differentiating the energy twice for any ab initio method.

The vibrational frequencies can be computed by determining the second derivatives of the potential energy with respect to the mass-weighted cartesian displacements in a system. This analytical method yields the quadratic force constants,  $f_{ij}$ , directly

$$f_{ij} = \left( \frac{\delta^2 V}{\delta q_i \delta q_j} \right)_{eq} \quad (2.6)$$

where  $q_i$  is the mass-weighted cartesian displacement defined in terms of the locations  $x_i$  of the nuclei relative to their equilibrium positions  $x_{i,eq}$  and their masses  $M_i$ :

$$q_i = M_i^{1/2} (x_i - x_{i,eq}) \quad (2.7)$$

In addition, the  $f_{ij}$  may be evaluated by numerical second differentiation

$$\frac{\delta^2 V}{\delta q_i \delta q_j} \cong \frac{\Delta(\Delta V)}{\Delta q_i \Delta q_j} \quad (2.8)$$



or by numerical first differentiation of analytical first derivatives<sup>58</sup>

$$\frac{\delta^2 V}{\delta q_i \delta q_j} \cong \frac{\Delta (\delta V / \delta q_i)}{\Delta q_j} \quad (2.9)$$

The frequencies calculated by Hartree-Fock methods are harmonic and the normal-mode vibrational frequencies are determined at the local minima points on the potential energy surface. In this work, the 6-31G\* SCF harmonic frequencies were calculated for the singlet ground and triplet excited states, using analytic second derivatives and then scaled by 0.9<sup>68</sup> to approximately correct for anharmonicity and the SCF procedure (neglect of electron correlation).



## Chapter 3

## Principles of Electronic Spectroscopy

## (I) Electronic Transitions

Transitions from one electronic state to those of another give rise to a band system. An oscillating electromagnetic field can induce a transition from vibronic states  $e''v''$  to  $e'v'$ ; the probability of this event per unit time and per unit radiation energy is given by<sup>69</sup>

$$W(e'v'e''v'') = \frac{8\pi^3}{3h} \left| M(e'v'e''v'') \right|^2 \quad (4.1)$$

where  $W(e'v'e''v'')$  is the Einstein probability coefficient and  $M(e'v'e''v'')$  is the transition moment

For electric dipole transitions the quantum mechanical transition moments have the form

$$M(e'v'e''v'') = \langle \psi_{e'v'} | \mu | \psi_{e''v''} \rangle \quad (4.2)$$

where  $\psi_{e'v'}$  and  $\psi_{e''v''}$  are the excited and ground state vibronic wave functions, respectively and  $\mu$  is the electric dipole operator.

The dipole moment can be resolved into two parts, one due to the electrons, the other due to the nuclei:

$$\mu = \mu_e(q) + \mu_N(Q) \quad (4.3)$$





where  $q$  and  $Q$  are the electronic and nuclear coordinates, respectively.

Within the Born-Oppenheimer approximation<sup>56</sup>, the molecular wavefunction  $\psi_{ev}$  for the  $v^{\text{th}}$  vibrational level of the  $e^{\text{th}}$  electronic state can be expressed as a product of an electronic and vibrational wavefunction.

$$\Psi_{ev} = \Psi_e(q, Q) \Psi_v(Q) \quad (4.4)$$

In this general case, the transition moment is given by

$$\begin{aligned} M(e'v' \rightarrow e''v'') = & \int \Psi_e'^* \mu_e \Psi_e'' d\tau_e \int \Psi_v'^* \Psi_v'' d\tau_v + \\ & \int \Psi_v'^* \mu_N \Psi_v'' d\tau_v \int \Psi_e'^* \Psi_e'' d\tau_e \end{aligned} \quad (4.5)$$

Since the electronic wavefunctions are orthogonal, the transition moment becomes<sup>70</sup>:

$$M(e'v' \rightarrow e''v'') = \int \Psi_e'^* \mu_e \Psi_e'' d\tau_e \int \Psi_v'^* \Psi_v'' d\tau_v \quad (4.6)$$

If equation (4.6) is zero for all components of the electric dipole operator  $\mu$ , then the transition between the states  $\psi_e'^*$  and  $\psi_e''$  is regarded as forbidden. Otherwise, the direct product of the factors  $\psi_e', \mu$  and  $\psi_e''$  must be totally symmetric, that is, symmetric to all operations of the point group appropriate to the equilibrium configurations of the



upper and lower molecular states since the limits on the integral span total space.<sup>71</sup> In group theoretical notation,

$$\Gamma\left(\psi_e^{ '*}\right) \otimes \Gamma\left(\mu_e\right) \otimes \Gamma\left(\psi_e^{ ''}\right) = \Gamma \text{ (Totally Symmetric)} \quad (4.7)$$

For a symmetry-allowed transition then, the condition placed on the electronic integrals of (4.6) is that

$$\Gamma\left(\psi_e^{ '*}\right) \otimes \Gamma\left(\psi_e^{ ''}\right) = \Gamma \text{ (x,y, or z)} \quad (4.8)$$

The low energy electronic transition in the C=O chromophore is the consequence of an  $n \rightarrow \pi^*$  electron promotion. The ground electronic configuration of formic acid can be written:

$$\dots (\sigma)^2 (\pi)^2 (n)^2 \qquad \widetilde{X}^1A'$$

Similarly, the electron configuration and the overall symmetry for the upper state can be expressed:

$$\dots (\sigma)^2 (\pi)^2 (n)^1 (\pi^*)^1 \qquad \widetilde{A}^1A''$$

Using these overall symmetries for the lower and upper states of HCOOH, the product in equation (4.8) in  $C_s$  symmetry transforms as  $\Gamma(z) = \Gamma(A'')$ . Thus, the transition is allowed by the electric selection rules, with the polarization of the electric dipole moment,  $\mu_e$ , along the z-axis (out-of-plane).



As a result, the electronic transition  $0_0^0$  is electric dipole allowed and should possess type C rotational contour. ( $M_m^n$  denotes a vibronic transition involving quanta  $n$  in the upper state and quanta  $m$  in the lower state and a level is designated as  $M^n$ .)

Besides the allowed electric dipole transition, the intensity in the  $n \rightarrow \pi^*$  system arises from vibrational-electronic coupling (Herzberg-Teller interaction). This involves the interaction between the motions of the electrons and the nuclei in polyatomic molecules<sup>72</sup>, resulting in a breakdown of the Born-Oppenheimer approximation<sup>56</sup>. With Herzberg-Teller coupling, the interaction of the electronic motion with vibration is no longer neglected so the electronic transition moment is not independent of nuclear motion. A Taylor series expansion of the electronic transition moment about the equilibrium nuclear configuration can be described:

$$M = M_e^0 \langle v' | v'' \rangle + \sum_i \frac{\delta M_e}{\delta Q_i} \langle v' | Q_i | v'' \rangle + \dots \quad (4.9)$$

The first term in the expansion represents another notation for  $M(e'v'e''v'')$  of equation (4.6).

In formic acid, transitions involving any number of quanta of  $a'$  frequencies,  $\nu_1$  to  $\nu_7$ , are allowed by the first term of the Herzberg-Teller expansion (4.9). These correspond to  $A'' \leftarrow A'$  transitions and should have type C contours



similar to the origin band. However, transitions involving odd quanta of the  $a''$  frequencies,  $\nu_8$  and  $\nu_9$ , are possible through the second term. The wavefunctions for these antisymmetric vibrations couple with the electronic wavefunction of the  $\tilde{A}^1A''$  state to form vibronic states of  $A'$  species. These forbidden transitions in the first order must borrow intensity from near-lying electronic transitions and appear as A/B hybrids. The possible vibronic transitions for the  $\tilde{A}^1A'' \leftarrow \tilde{X}^1A'$  electronic transition of formic acid are given in Figure 6.

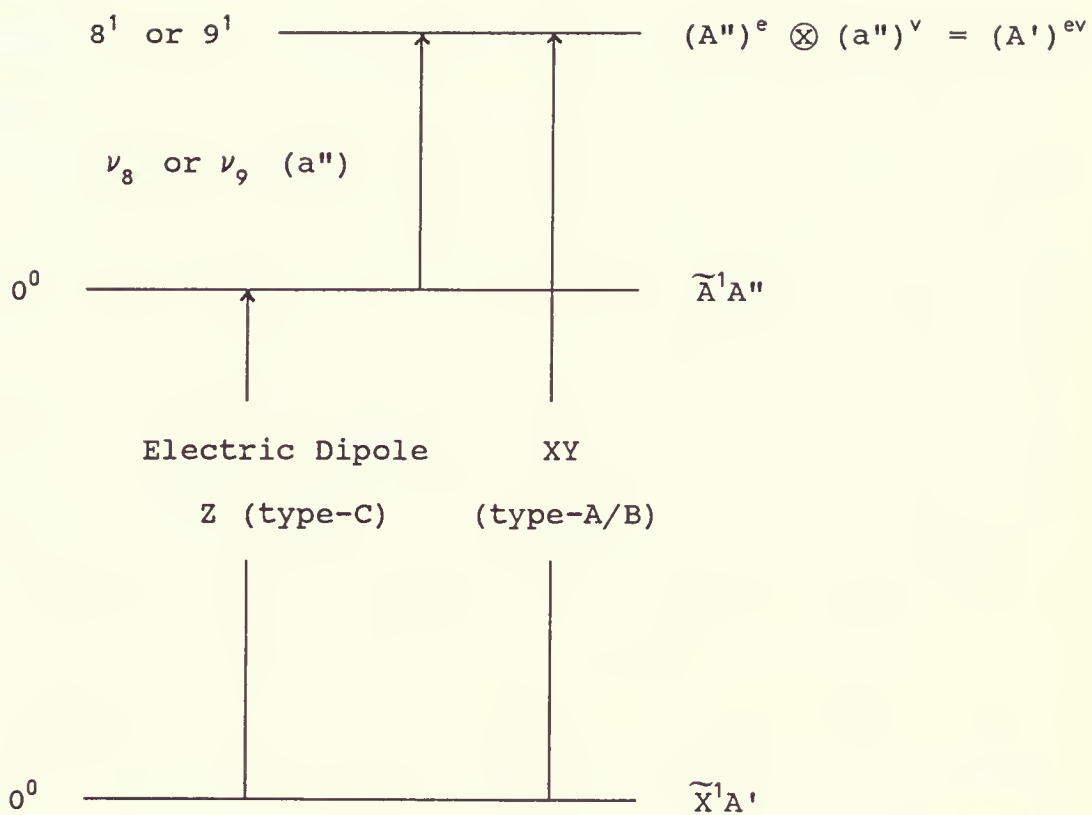
Although the transition is predominantly allowed as electric dipole radiation, the transition is also magnetic dipole and electric quadrupole allowed. In quantum theory, the transition probability produced by magnetic dipole or electric quadrupole radiation is obtained by substituting the magnetic dipole or electric quadrupole moment for the electric dipole moment in the transition moment equation (4.2). A non-zero value for this probability results if the product  $\psi_e' * \psi_e''$  has the same species as one of the components of the magnetic dipole or electric quadrupole moments. The components of the magnetic dipole moment behave as the three rotations  $R_x$ ,  $R_y$ , and  $R_z$  and the electric quadrupole moment behaves in the same way as the components of the polarizability.<sup>70</sup> The species for the rotations and the products of two translations are given in Table 3 for the  $C_s$  point group.





Figure 6  
Possible vibronic transitions in the  $\tilde{A}^1A'' \leftarrow \tilde{X}^1A'$   
electronic transition of HCOOH







Lastly, the transition is allowed by the spin selection rule. In equation (4.2) the transition moment excluded the spin of the states; however, the full electronic eigenfunction must take account of the fact that each electron has a spin  $s=1/2$  which can orient itself parallel or antiparallel to any preferred direction. As long as the coupling of the individual spins with the orbital motion is small, the spins of the individual electrons forms a resultant spin  $S$ , and the electronic eigenfunction can be written as a product of an orbital,  $\psi_e$  and a spin function.<sup>70</sup> The transition moment then can vanish for states of different spin since the spin functions corresponding to different  $S$  values would be orthogonal. As the ground state and the lowest lying excited state of formic acid are of the same multiplicity, singlet, the intercombination is also formally spin allowed.

## (II) Vibrational Structure

The intensity of a spectroscopic transition between vibronic states depends upon the value of  $|M|^2$  in equation (4.1). In the first approximation of equation (4.6) for  $M$ , the second integral representing the electronic transition moment is considered a constant.<sup>69</sup> The condition for the validity of the Born-Oppenheimer approximation<sup>56</sup> is that the electronic wavefunctions vary slowly with  $Q$ ; otherwise, the electrons would not be able to adjust fast enough to follow



the nuclear motion. It follows that the integral should also vary only slightly with  $Q$ . Thus, neglecting the dependence of  $\psi_e$  on the nuclear coordinates, the integral can be replaced by a constant corresponding to a configuration of the nuclei near the equilibrium position of one of the two electronic states. With this approximation, the transition probability, which is proportional to the magnitude of  $M^2$  can be resolved into a factor depending on the nuclear motion alone and a factor depending on the electronic motion alone. From this discussion, the first factor of equation (4.6) becomes important and certain vibrational transitions make the total transition moment  $M(e'v'e''v'')$  different from zero.

In particular, for polyatomic molecules, transitions from various vibrational levels of one electronic state to another give rise to a band system. Moreover, as several vibrations are involved, the vibrational structure is generally complicated. Therefore, the intensities of the vibrational bands in an electronic transition depend on the vibrational overlap integral described above.

To understand the differences in the intensities of different vibrational transitions, the Frank-Condon principle<sup>74</sup> must be applied. According to this principle, the relative intensities of the vibrational bands of an electronic transition depend on the changes in the geometrical structure due to electronic excitation. If the potential





functions in the two electronic states are nearly alike, giving rise to similar internuclear distances and vibrational frequencies, then the vibrational overlap integral will be different from zero only if none of the vibrational quantum numbers change. In this case,  $\Delta\nu_i=0$  for all vibrational quantum numbers. There would be one band of outstanding intensity, the 0-0 band, followed by sequence bands. If on the other hand, the equilibrium position of the nuclei changes in going from one electronic state to another and if this change is most nearly represented by the vibrational mode  $\nu_i$ , bands with  $\Delta\nu_i \neq 0$  will occur strongly. If the equilibrium position change is large, the maximum intensity is no longer at  $\nu_i'=0$ . Qualitatively, the vibrational modes which are associated with structural changes will be active in the spectrum forming progressions.

In general, the excited state geometry for a polyatomic molecule differs from that of the ground state. For the electronic excitation of the  $n \rightarrow \pi^*$  type, an electron is placed in an antibonding orbital,  $\pi^*$ , which has a higher energy than the  $n$  nonbonding orbital. The molecule tends to minimize this excess energy by rearranging its structure to decrease the antibonding character and to achieve stability. As expressed in Walsh's rules<sup>75</sup>, if an antibonding  $p$  atomic orbital is converted to an  $s$  atomic orbital, then the energy should diminish. In molecules with the carbonyl chromophore,



this can be accomplished by distorting the molecule from a planar to nonplanar configuration. As the molecule distorts from the plane, the  $\pi$  orbital changes from a pure p atomic orbital on the carbon centre to an  $sp^3$  hybrid orbital. This behaviour is expected for formic acid, giving rise to deformation of the planar structure. In addition, the C=O bond should extend.

A nonplanar molecule can be characterized by two distinct equilibrium configurations which are related to each other by an inversion of the nuclei at the centre of mass. The potential function for the out-of-plane displacement of an atom in formic acid would have a double minimum, with a central barrier expressing the stability of the molecule as distortion occurs. Figure 7 shows the correlation of the energy levels for a planar, slightly nonplanar and rigidly nonplanar molecule. The potential energy<sup>76</sup> for the out-of-plane vibration can be described by:

$$V(Q) = \frac{Q^2}{2} + A e^{(-a^2 Q^2)} \quad (4.10)$$

where  $Q$  is the normal coordinate and  $A$  and  $a$  are constants which depend upon a scaling factor, a shape factor and the reduced barrier height for the function.



Figure 7  
Correlation diagram for the energy levels of  
rigidly planar and flexible nonplanar structures



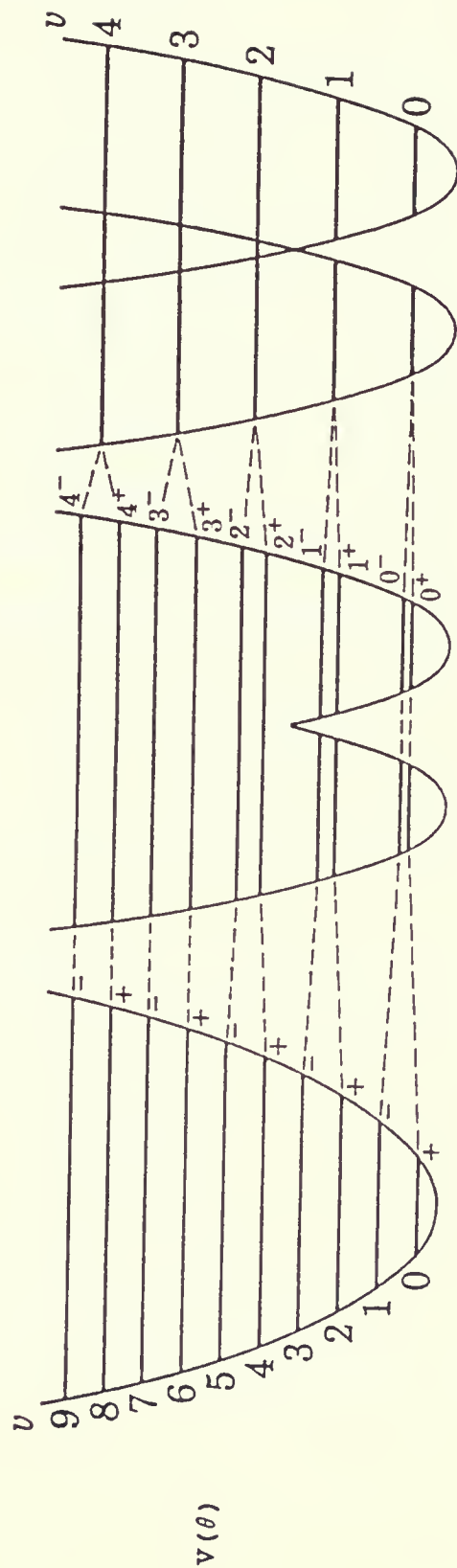
# INTERMEDIATE

BARRIER

NO BARRIER

INFINITE

BARRIER



$$\frac{-}{-} \quad \frac{0}{0} \quad \frac{+}{+}$$

$\theta$

$$\frac{-}{-} \quad \frac{0}{0} \quad \frac{+}{+}$$

$\theta$

$$\frac{-}{-} \quad \frac{0}{0} \quad \frac{+}{+}$$

$\theta$





## (III) Rotational Structure

Each of the vibronic bands of an electronic system has a fine structure which is due to the transitions between the various rotational quantum states of vibronic levels. This fine structure, if resolvable is often complex.

For a three-dimensional rigid body such as a molecule, the rotation is resolved into rotational components about three mutually perpendicular principal axes through the centre of mass for the system. A body then, has three principal moments of inertia,  $I_a$ ,  $I_b$ , and  $I_c$ ; one about each axes where  $I_a < I_b < I_c$  by convention. By definition<sup>77</sup>,

$$I_j = \sum_{i=1}^N m_i r_i^2 \quad (4.11)$$

where  $r_i$  is the perpendicular distance from mass  $m_i$  to the  $j$  axis.

From these moments of inertia a set of rotational constants describing an electronic state can be evaluated:

$$\begin{aligned} A &= (h/8\pi^2 c I_a) \\ B &= (h/8\pi^2 c I_b) \\ C &= (h/8\pi^2 c I_c) \end{aligned} \quad (4.12)$$

where  $h$  is Planck's constant

$c$  is the velocity of light

and  $I_a, I_b$  and  $I_c$  are the principal moments of inertia



The rotational energy<sup>69</sup> of an asymmetric rotor is given by

$$F(J,K) = \frac{1}{2}(A+C)J(J+1) + \frac{1}{2}(A-C)E(K) \quad (4.13)$$

where  $J$  is the quantum number associated with the total angular momentum and  $\kappa$  is the asymmetry parameter. The parameter describing the degree of asymmetry is presented as

$$K = \frac{(2B - A - C)}{A - C} \quad (4.14)$$

When  $B=C$  and  $\kappa=-1$ , the expression becomes that for a prolate symmetric rotor. The energy is represented by

$$F(J,K) = \bar{B}J(J+1) + (A - \bar{B})K^2 \quad (4.15)$$

where  $\bar{B} = (B+C)/2$

and  $K$  is the quantum number for the component of the angular momentum along the top (internuclear) axis, a axis.

In the ground state, formic acid is a near-prolate symmetric top. For asymmetric top molecules, the selection rules,  $\Delta J=0, \pm 1$  and  $\Delta K=0, \pm 1$  apply. The selection rule for the quantum number  $J$  leads to the three branches P, Q and R in the rotational structure of a band. For an A-type band,  $\Delta K=0$  which corresponds to a parallel component of the transition moment for the electronic transition. For the B and C-type



bands,  $\Delta K = \pm 1$  giving a component perpendicular to the top axis. To compute a rotational band contour in the asymmetric rigid rotor approximation, a computer program called Parkin<sup>78</sup> was utilized.

The rotational constants for the excited state of formic acid are expected to be different from the ground state values. In this study, estimates of  $A'$ ,  $B'$  and  $C'$  have been made by choosing the calculated asymmetric top contours for type A, type B and type C bands that most closely represent the observed  $K$  subband heads and the  $J$  structure of the rotational spectrum of the  $O_0^0$  band. The planarity or nonplanarity of the molecule can be expressed in terms of the inertial defect

$$\Delta = 16.858 \left( \frac{1}{C} - \frac{1}{A} - \frac{1}{B} \right) \text{amu}\text{\AA}^2 \quad (4.16)$$

For the computation, the maximum  $K$  value was 15 and the transitions were calculated up to a  $J$  value of 50. The ground state rotational constants and the centrifugal distortion constants used were those determined by Bellet et al.<sup>15</sup> In addition, the excited state rotational constants evaluated by Ng and Bell<sup>48</sup> were preliminarily used. From the symmetric top approximation, the  $K$  numbering for the theoretical C-type band using the above values was decided and compared to the



experimental contour for the  $^PQ$  branches which appear as the main head forming features. From this point, the procedure outlined by Ng and Bell<sup>48</sup> was followed to approximate the values of the excited state rotational constants. From the K numbering a plot of the K subband spacing versus K could be made for the experimental contour. This graph should be a straight line with slope  $2\Delta A - 2\Delta \bar{B}$  where  $\Delta A = A' - A''$ ,  $\Delta \bar{B} = \bar{B}' - \bar{B}''$ , and  $\bar{B} = (B + C)/2$ . To estimate  $\Delta \bar{B}$ , the spacing of the J lines in a P branch of a particular K subband in the experimental spectrum was considered. The spacing is given by  $2\Delta \bar{B}J - 2\bar{B}''$ . The observed J lines were approximately equally spaced and corresponded to  $J \approx 15$ . From this value and the slope of the above plot, a value for A' was found. Approximate values of B' and C' were obtained from the asymmetry parameter. Type A, type B and type C contours were next calculated while slightly adjusting the rotational constants until the contours corresponded as close as possible to the experimental rotational contour.





## CHAPTER 4

### EXPERIMENTAL

#### (I) Fluorescence Spectroscopy

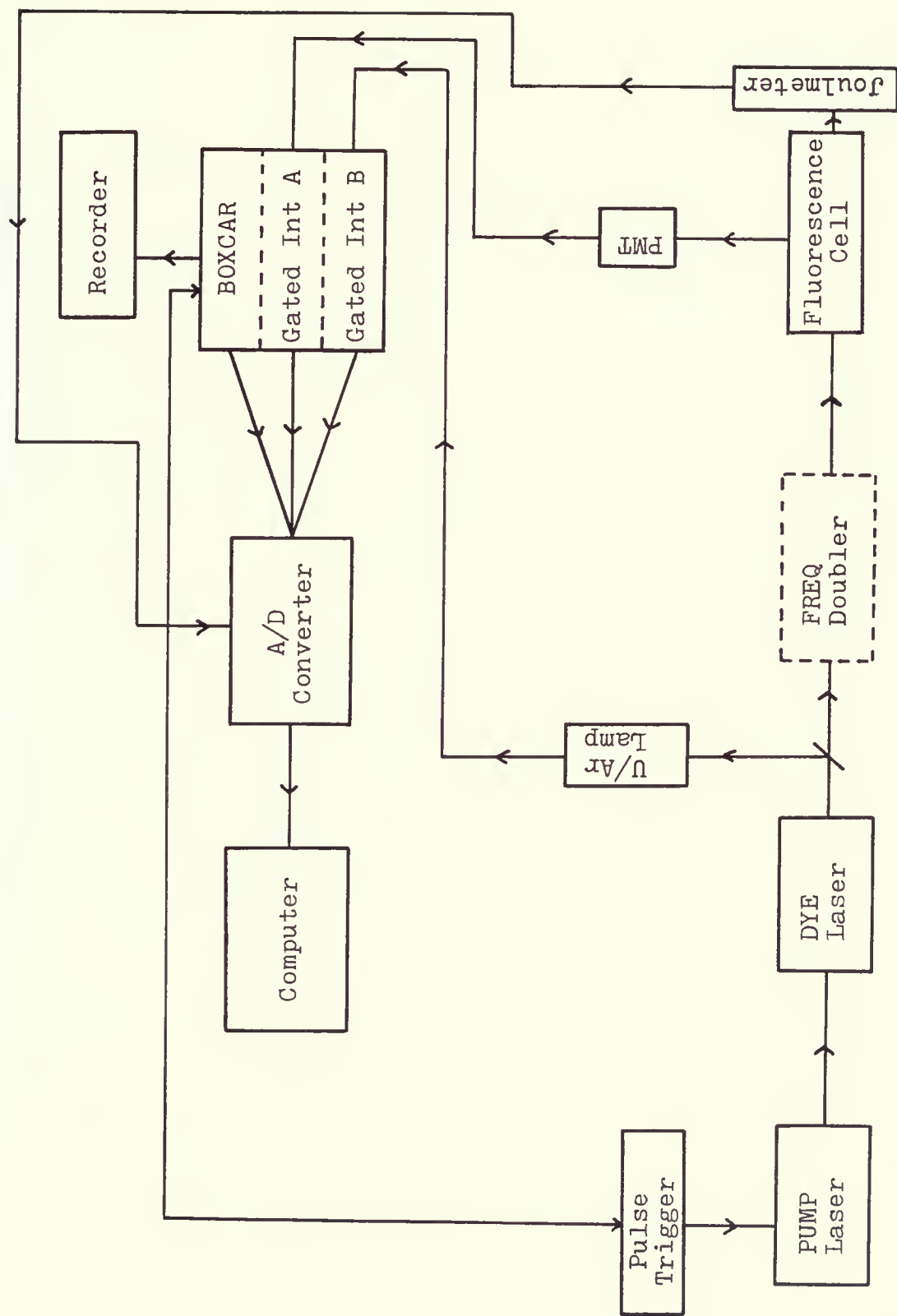
Fluorescence spectroscopy is based on the emission of radiation by a sample. Lasers provide a selective means for populating excited states, and the study of spectra generated by the emission of radiation as these states decay is known as laser-induced fluorescence.<sup>79</sup> A block diagram of the instrumentation used for the laser-induced fluorescence studies of formic acid is given in Figure 8.

The laser-induced fluorescence (LIF) excitation spectra of gas phase HCOOH (Aldrich, 96%), DCOOH (MSD Isotopes, 98.8 atom %D), HCOOD (MSD Isotopes, 98.1 atom %D) and DCOOD (MSD Isotopes, 98.9 atom %D) were recorded in a slow flow system at 60<sup>0</sup> C. The samples were degassed by freeze-pump-thaw cycles prior to experimentation. A pulsed (20 Hz) HyperVAG-750 Nd:YAG laser operating at the third harmonic, 355 nm, was used to pump a Hyperdye-300 grazing incidence dye laser, producing tunable radiation in the region of 580-490 nm with Coumarin 540A and 500 (Exciton) laser dyes. The dye laser output was frequency doubled (HyperTRAC-1000) by angle-tuned, temperature stabilized crystals, KD\*P (265-280 nm) or KB5 (250-265 nm), and directed to a 20-cm pyrex T-cell equipped with quartz windows and a series of light baffles to minimize



Figure 8  
Schematic diagram of the instrumentation  
for Laser-induced fluorescence







scattered light. The fluorescence cell contained 1 Torr of formic acid and the cell pressures for the isotopes were typically 0.2-0.8 Torr. Figure 9 depicts the path of the laser beam through the fluorescence cell compartment. The spectral linewidth of the laser beam was about  $0.1\text{ cm}^{-1}$ .

Emission was collected at right angles to the excitation source and detected with a cooled photomultiplier (EMI 9816QB). A 350 nm cutoff filter was placed immediately before the photomultiplier to discriminate against the excitation source. Signals from the photomultiplier tube were processed by a gated integrator (EG&G PAR Model 162) before digitization. The spectra were obtained at increment rates of 0.25 and  $0.05\text{ cm}^{-1}$ . The fluorescence spectra were recorded digitally using a homebuilt data acquisition system described by Rutherford et al.<sup>80</sup> All the data was acquired and processed using an IBM PC. A photograph of the experimental set-up in the laboratory is shown in Figure 10.

The laser power was simultaneously monitored using a commercial joulemeter (Molelectron Model J305) positioned after the fluorescence cell. For the spectra in the region  $37300\text{--}40500\text{ cm}^{-1}$ , the intensity signal of the laser was constant, but insufficient in comparison to the weak emission to give properly ratioed spectra. Similarly, the spectrum of formic acid in the region  $35900\text{--}37500\text{ cm}^{-1}$  has not been corrected for laser intensity. Due to a noisy and greatly fluctuating power





Figure 9  
Diagram of the optical light path through  
the fluorescence excitation cell



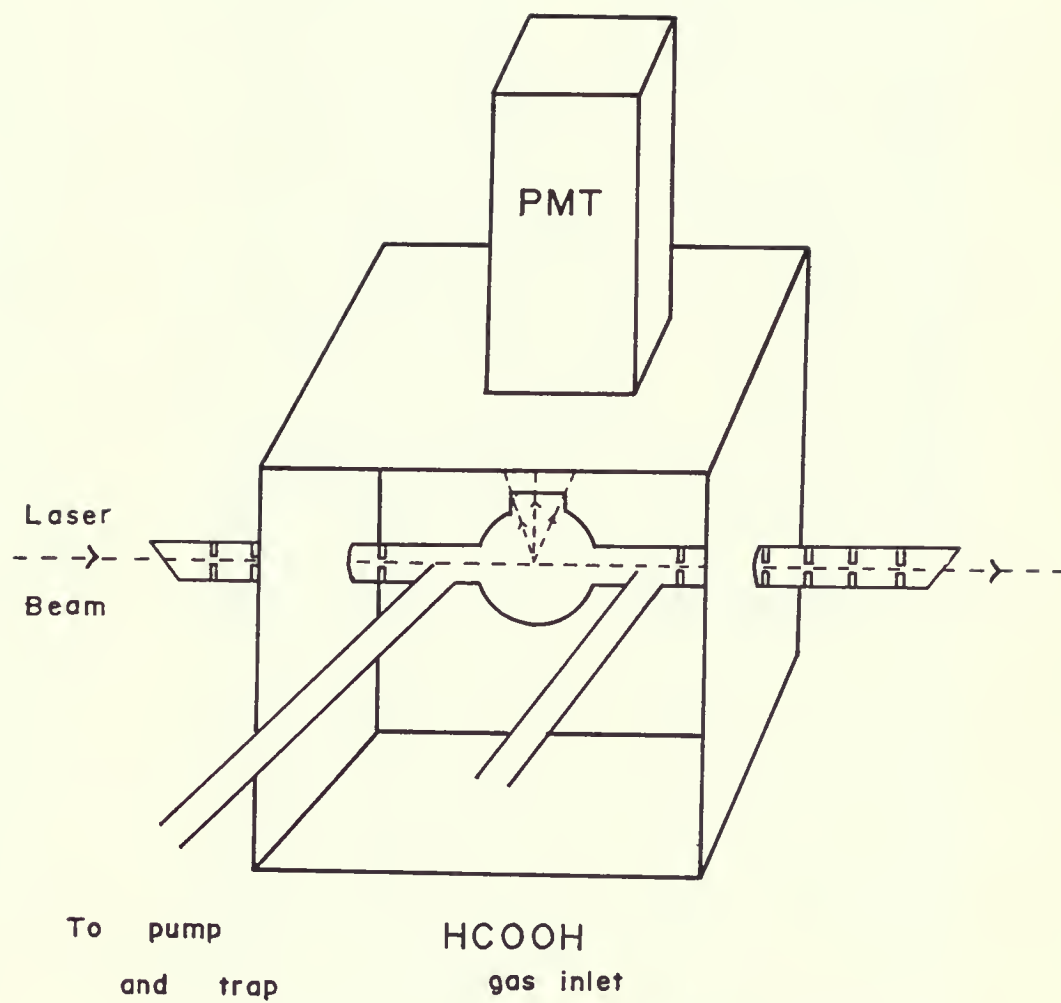




Figure 10  
Photograph of the experimental set-up  
in the laboratory for  
fluorescence spectroscopy









spectrum, normalization introduces distortion in the spectrum.

An optogalvanic spectrum of an Ar filled uranium hollow-cathode lamp excited by the dye laser fundamental was also simultaneously recorded and served as a reference for calibration of the excitation spectra. A portion of the laser beam was diverted by use of a beamsplitter and focused onto the discharge region of the hollow-cathode lamp. This method of frequency calibration makes use of the optogalvanic effect. When the frequency of the laser corresponds to an atomic transition of a species in the discharge, a change in the population of metastable states is produced and detected by measuring the voltage changes across the discharge tube.<sup>81</sup> The observed uranium and argon lines were assigned using the UV-visible reference lines catalogued in the M.I.T. Wavelength Tables.<sup>82</sup> The reference wavelength data versus the nominal laser wavelength were fitted to a third-degree polynomial using the data manipulation routines accompanying the data acquisition system. From this equation, the calibrated wavelengths for the fluorescence excitation spectra were calculated. Furthermore, an ASCII file representing the calibrated spectrum as X-Y pairs of numbers was created, using the data acquisition options to produce plots of the fluorescence spectra with the HP LaserJet Series II printer and the software package, Sigmaplot.

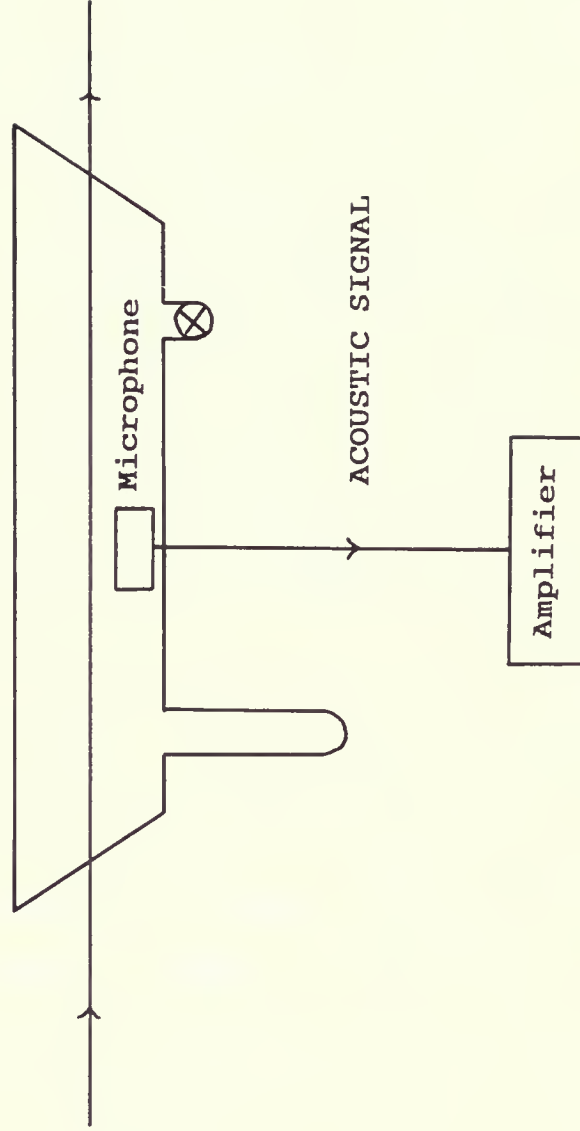


Figure 11  
Schematics of the Photoacoustic cell



SAMPLE CELL

MODULATED  
RADIATION





### (III) Supersonic Jet Spectroscopy

When a gas expands from a high-pressure tank through a properly defined orifice into a low-pressure discharge chamber, a supersonic jet emerges in which the thermal energy originally present becomes converted into a directed mass flow.<sup>85</sup> This rapid expansion into a vacuum cools the molecules to low temperatures and depopulates the rotational levels leading to a simplified molecular spectra.<sup>84</sup> Supersonic jets can be used as a source for gas phase molecular spectroscopy. Figure 12 shows the supersonic jet apparatus used for the HCOOH experiments. A laser beam is crossed with a jet as a means for exciting molecular fluorescence.

Attempts to obtain the supersonic jet spectrum of formic acid were unsuccessful. The pressures in the 20 cm x 20 cm vacuum chamber were maintained in the range of  $10^{-4}$ - $10^{-3}$  Torr utilizing a mechanical booster (Edwards EH500) and a high vacuum pump (Edwards E2M80). The nozzle was 0.3 mm in diameter and placed 10 nozzle diameters from the laser source. The 355 nm third harmonic of the Nd:YAG laser was used to pump the dye laser operated on Coumarin 500 (536-490 nm) (Exciton). Frequency doubled output was generated with a KD\*P crystal and harmonic separator, similar to the LIF experiments. The laser beam entered and exited the chamber through 15-cm baffle arms equipped with Brewster windows. Emission was detected



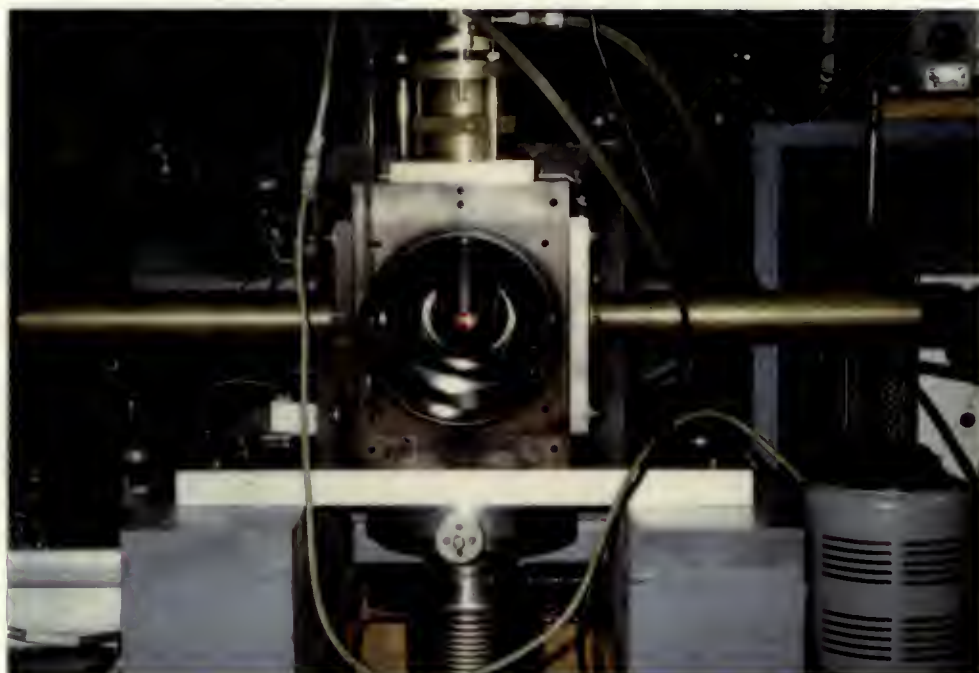


Figure 12  
Description of the cell compartment set-up  
used for supersonic jet spectroscopy

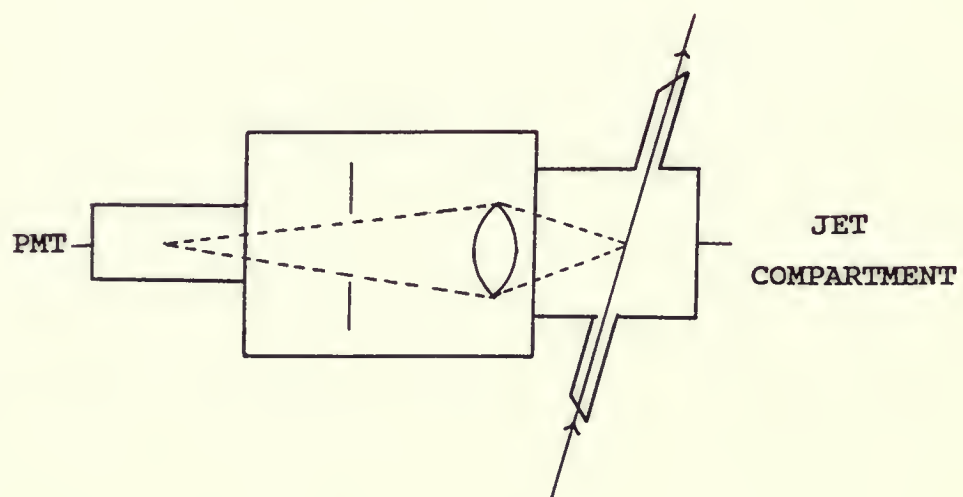
- A) Photograph of the nozzle and vacuum chamber
- B) Laser path in the supersonic jet (top view)



(A)



(B)





at 90 degrees to both the jet and the laser beam with a cooled photomultiplier (EMI 9816QB). A 350 nm filter was placed immediately before the photomultiplier to discriminate against the excitation source. Signals from the photomultiplier were processed with a gated integrator/boxcar averager (PAR 162) and displayed on a stripchart recorder. For the experiment, argon was saturated with formic acid by bubbling Ar through approximately 1 cm of HCOOH liquid kept at 0°C. Benzene was preliminarily utilized as a standard at 0°C to optimize the optical alignment of the supersonic jet. Maintaining the formic acid sample at room temperature and modifying the carrier gas to helium also did not improve the weak signal; therefore, the supersonic jet spectrum of HCOOH could not be recorded.

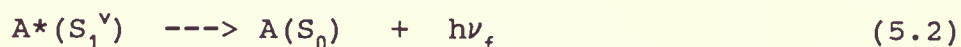
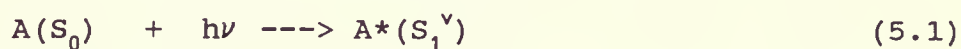


## CHAPTER 5

## RESULTS AND DISCUSSION

## (I) Fluorescence Excitation Spectra

Fluorescence results from a molecular system being excited into an upper state by absorption of radiation and then decaying back to a lower state.<sup>86</sup> In particular, the electronic transition,  $n \rightarrow \pi^*$ , in the carbonyl chromophore of a molecule, such as formic acid, involves the promotion of the system to the excited electronic state  $S_1$ . The emission of radiation from this singlet state to the ground electronic  $S_0$  state, a spin and symmetry allowed transition for HCOOH, describes the phenomenon of fluorescence. The main processes which occur are excitation (5.1) followed by fluorescence (5.2):



where the \* refers to the electronically excited molecule and  $v$ , the excited vibronic state.

In this work, a laser has been used to induce the fluorescence of formic acid from the  $S_1$  state. From these studies the lifetime of formic acid in the  $S_1$  state has been estimated to be 10-20 ns. Figures 13-16 show the laser





Figure 13  
Laser induced fluorescence excitation spectrum  
of formic acid,  $\text{HCOOH}$  from  $37300 - 40500 \text{ cm}^{-1}$

Experimental Conditions:

- A)  $0.25 \text{ cm}^{-1}$  resolution
- B) 1 Torr pressure
- C)  $60^{\circ} \text{ C}$



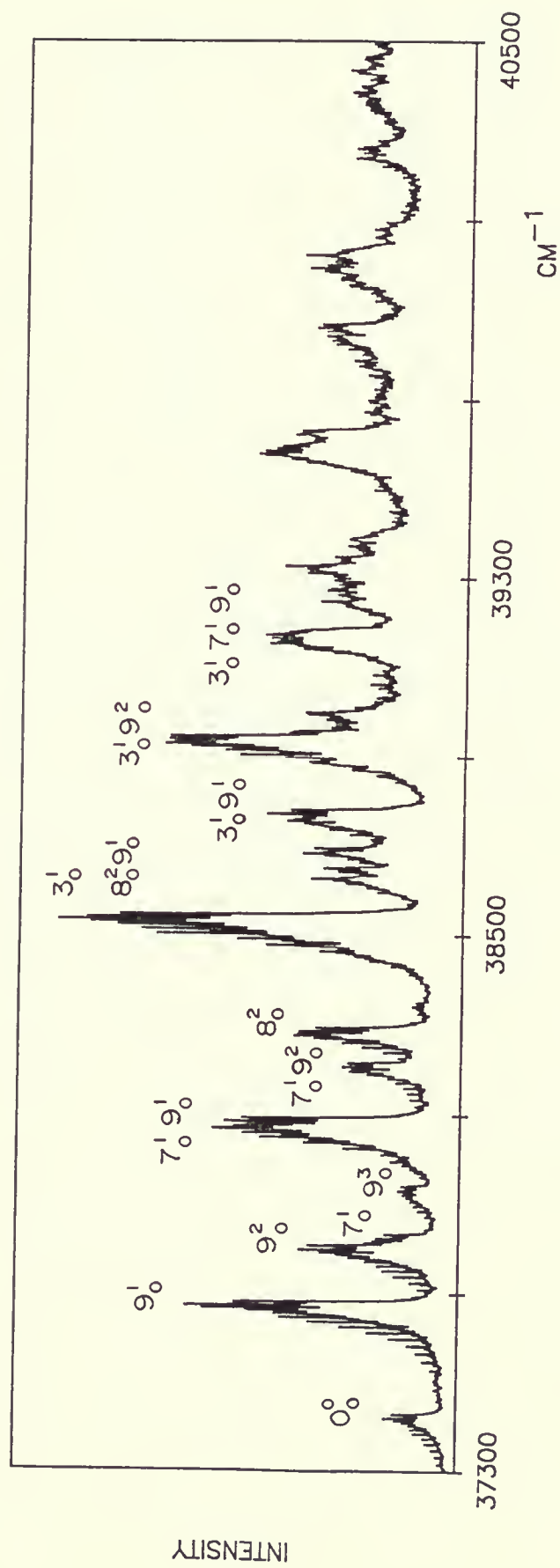
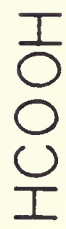




Figure 14  
Laser induced fluorescence excitation spectrum  
of formic acid,  $\text{HCOOD}$  from  $37300 - 40500 \text{ cm}^{-1}$

Experimental Conditions:

- A)  $0.25 \text{ cm}^{-1}$  resolution
- B) 0.8 Torr pressure
- C)  $60^{\circ} \text{ C}$



# HCOOD

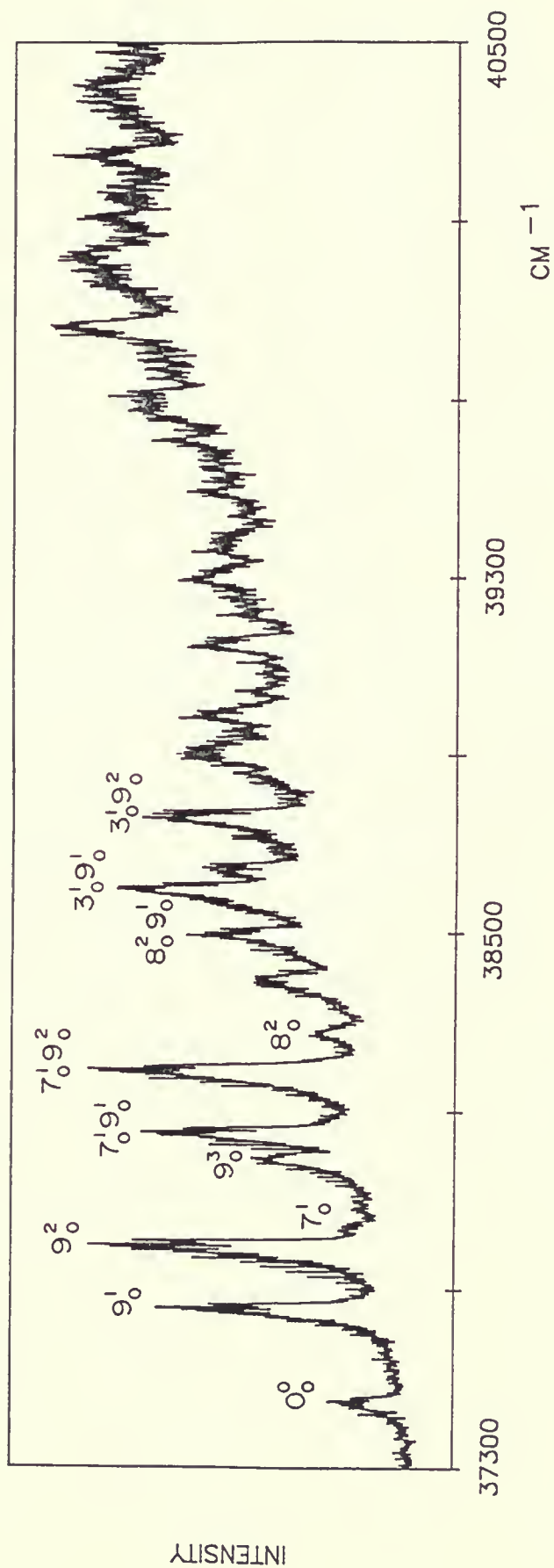






Figure 15  
Laser induced fluorescence excitation spectrum  
of formic acid, DCOOH from 37300 - 40500  $\text{cm}^{-1}$

Experimental Conditions:

- A) 0.25  $\text{cm}^{-1}$  resolution
- B) 0.5 Torr pressure
- C) 60<sup>0</sup> C



DCOOH

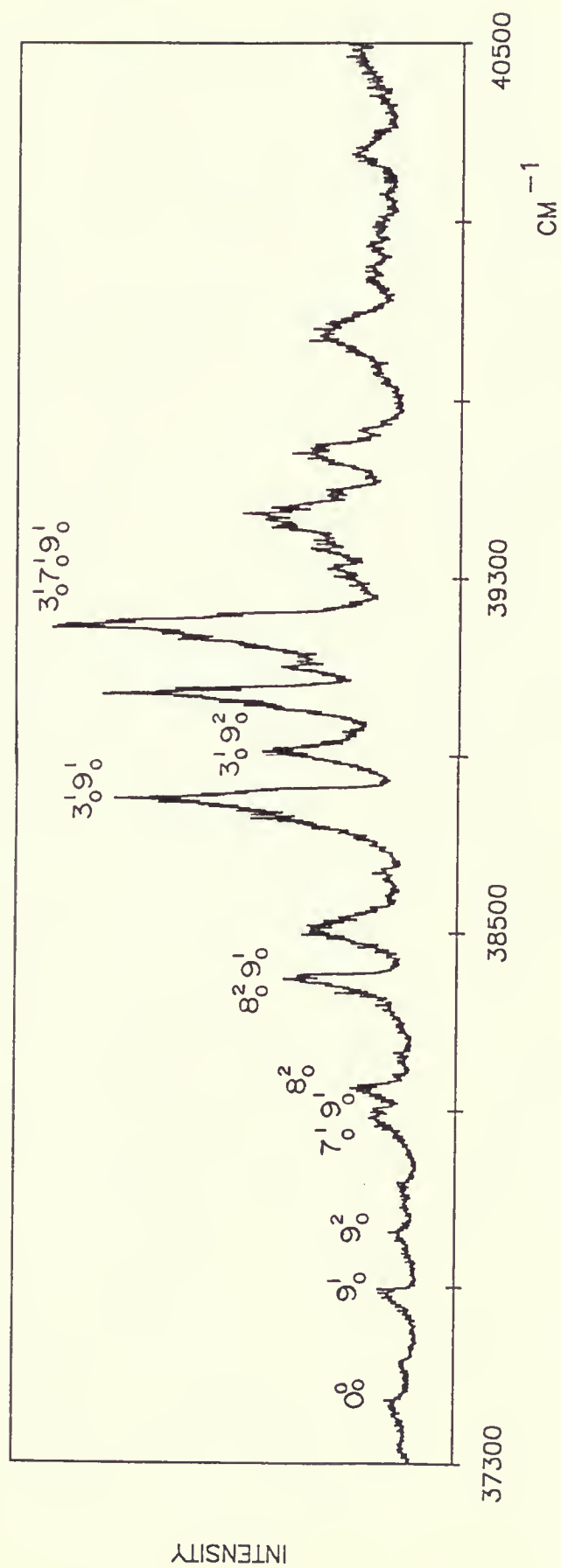




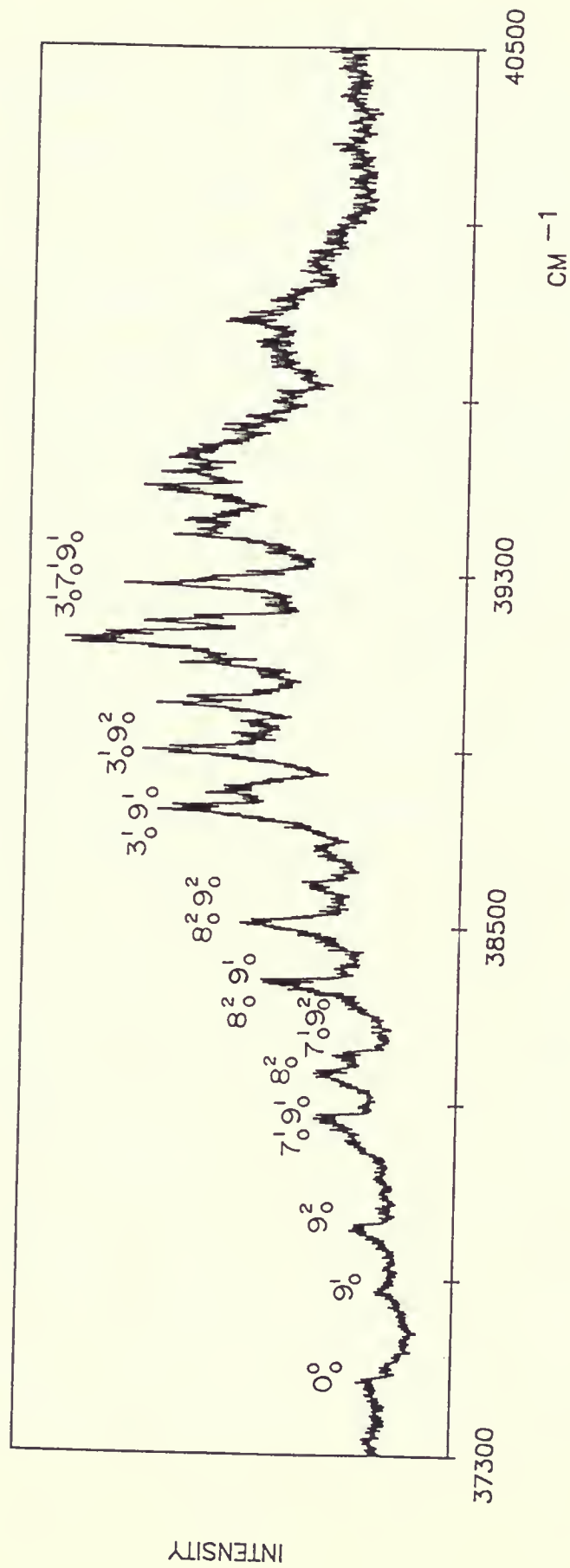
Figure 16  
Laser induced fluorescence excitation spectrum  
of formic acid, DCOOD from 37300 - 40500  $\text{cm}^{-1}$

Experimental Conditions:

- A) 0.25  $\text{cm}^{-1}$  resolution
- B) 0.2 Torr pressure
- C) 60<sup>0</sup> C



# DCOOD







induced fluorescence excitation spectra of the four isotopomers of formic acid in the UV region (268-246 nm). In addition, the 278-266 nm laser excitation spectrum of HCOOH has been recorded and is depicted in Figure 17. Tables 6 and 7 collect the wavenumbers of the observed band heads. The strongest band in the latter region has a sharp K-type rotational fine structure. This band was recorded at a higher resolution than the former spectra: the rotational spectrum obtained is given in Figure 18. Table 8 lists the wavenumbers of the proposed  ${}^PQ_k$  heads. Calibration plots corresponding to all these spectra are produced in Figure 19. As a brief overview, the spectra of HCOOH and HCOOD are remarkably clear at the long wavelength end and the bands show an open K-type rotational fine structure. The corresponding spectra of the species, DCOOH and DCOOD, are weaker and hence are somewhat less well defined.

From the high resolution study of Ng and Bell<sup>48</sup>, the rotational contour of the band at  $38546\text{ cm}^{-1}$  was synthesized as a hybrid composed of A, B and C type bands with intensity ratios 1:1:2. The presence of a strong C type component means that the near UV system is electric dipole allowed as previously discussed (Section 2.1) and can be given the assignment  $0_0^0$ . This absorption system was attributed to the  $n \rightarrow \pi^*$  electronic transition in the carbonyl group of formic acid. The starting point for the analysis of the emission



Figure 17

Laser induced fluorescence excitation spectrum  
of formic acid,  $\text{HCOOH}$  from  $35900 - 37500 \text{ cm}^{-1}$

Experimental Conditions:

- A)  $0.25 \text{ cm}^{-1}$  resolution
- B) 1 Torr pressure
- C)  $60^{\circ} \text{ C}$



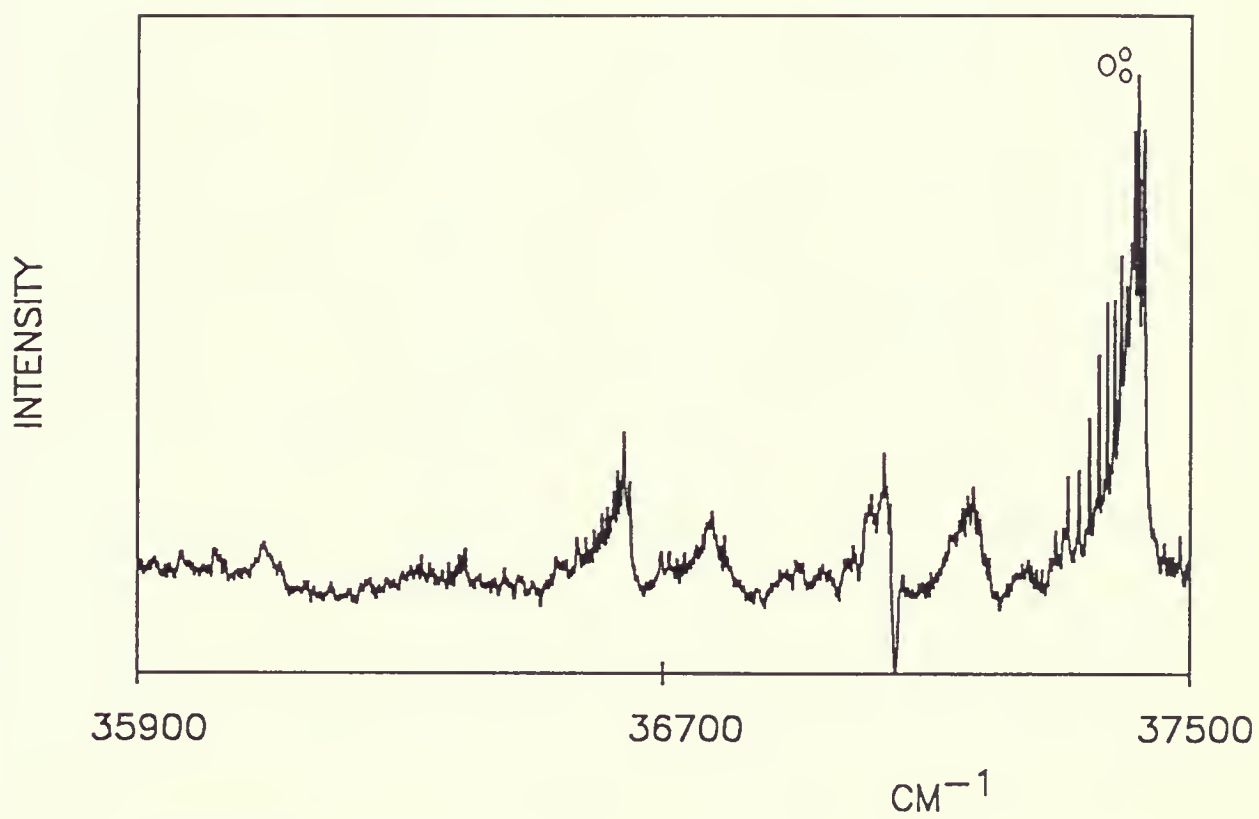




TABLE 6: OBSERVED BAND HEADS<sup>a</sup> IN THE EXCITATION SPECTRA OF FORMIC ACID:

HCOOH, HCOOD

assign.	mode	HCOOH		HCOOD	
		position	displacement	position	displacement
$0^0_0$	origin	37431.5	0.0	37461.5	0.0
$9^1_0$	(O-H oop) <sup>b</sup>	37682.7	251.2	37670.0	208.5
$9^2_0$		37810.2	378.7	37812.5	351.0
$7^1_0$	(O=C=O)	37835.4	403.5	37854.0	392.5
$9^3_0$		37945.1	513.6	38007.8	546.3
$7^1_0 9^1_0$		38094.8	663.3	38065.6	604.1
$7^1_0 9^2_0$		38218.3	786.8	38207.8	746.3
$8^2_0$	(C-H oop)	38296.9	865.4	38295.1	833.6
$3^1_0$	(C=O)	38546.7	1115.2	—	—
$8^2_0 9^1_0$		38546.7	1115.2	38512.4	1050.9
$3^1_0 9^1_0$		38781.8	1350.3	38612.4	1150.9
$3^1_0 9^2_0$		38950.6	1519.1	38774.6	1313.1

a) measurements, in  $\text{cm}^{-1}$ , were taken at the high frequency edge of the band.

b) the  $9^1$  level is calculated to lie below the equilibrium position of the syn conformation and would not be split into a (+) - (-) inversion doublet.





TABLE 7: OBSERVED BAND HEADS<sup>a</sup> IN THE EXCITATION SPECTRA OF FORMIC ACID:

DCOOH, DCOOD

assign.	mode	DCOOH		DCOOD	
		position	displacement	position	displacement
0 <sup>0</sup> <sub>0</sub>	origin	37445.5	0.0	37479.3	0.0
9 <sup>1</sup> <sub>0</sub>	(O-H oop) <sup>b</sup>	37698.1	252.6	37685.2	205.9
9 <sup>2</sup> <sub>0</sub>		37828.1	382.6	37829.6	350.3
7 <sup>1</sup> <sub>0</sub> 9 <sup>1</sup> <sub>0</sub>		38106.3	660.8	38077.0	597.7
8 <sup>2</sup> <sub>0</sub>	(C-H oop)	38160.5	715.0	38181.5	702.2
7 <sup>1</sup> <sub>0</sub> 9 <sup>2</sup> <sub>0</sub>		—	—	38223.0	743.7
8 <sup>2</sup> <sub>0</sub> 9 <sup>1</sup> <sub>0</sub>		38408.3	962.8	38385.7	906.4
3 <sup>1</sup> <sub>0</sub> 9 <sup>1</sup> <sub>0</sub>		38825.5	1380.0	38776.0	1296.7
3 <sup>1</sup> <sub>0</sub> 9 <sup>2</sup> <sub>0</sub>		38938.5	1493.0	38913.3	1434.0

a) measurements, in cm<sup>-1</sup>, were taken at the high frequency edge of the band.

b) the 9<sup>1</sup> level is calculated to lie below the equilibrium position of the syn conformation and would not split into a (+) - (-) inversion doublet.



Figure 18  
The rotational spectrum of the  $0^0_0$  band of HCOOH  
recorded at 1 Torr,  $60^0$  C, and  
0.05  $\text{cm}^{-1}$  resolution



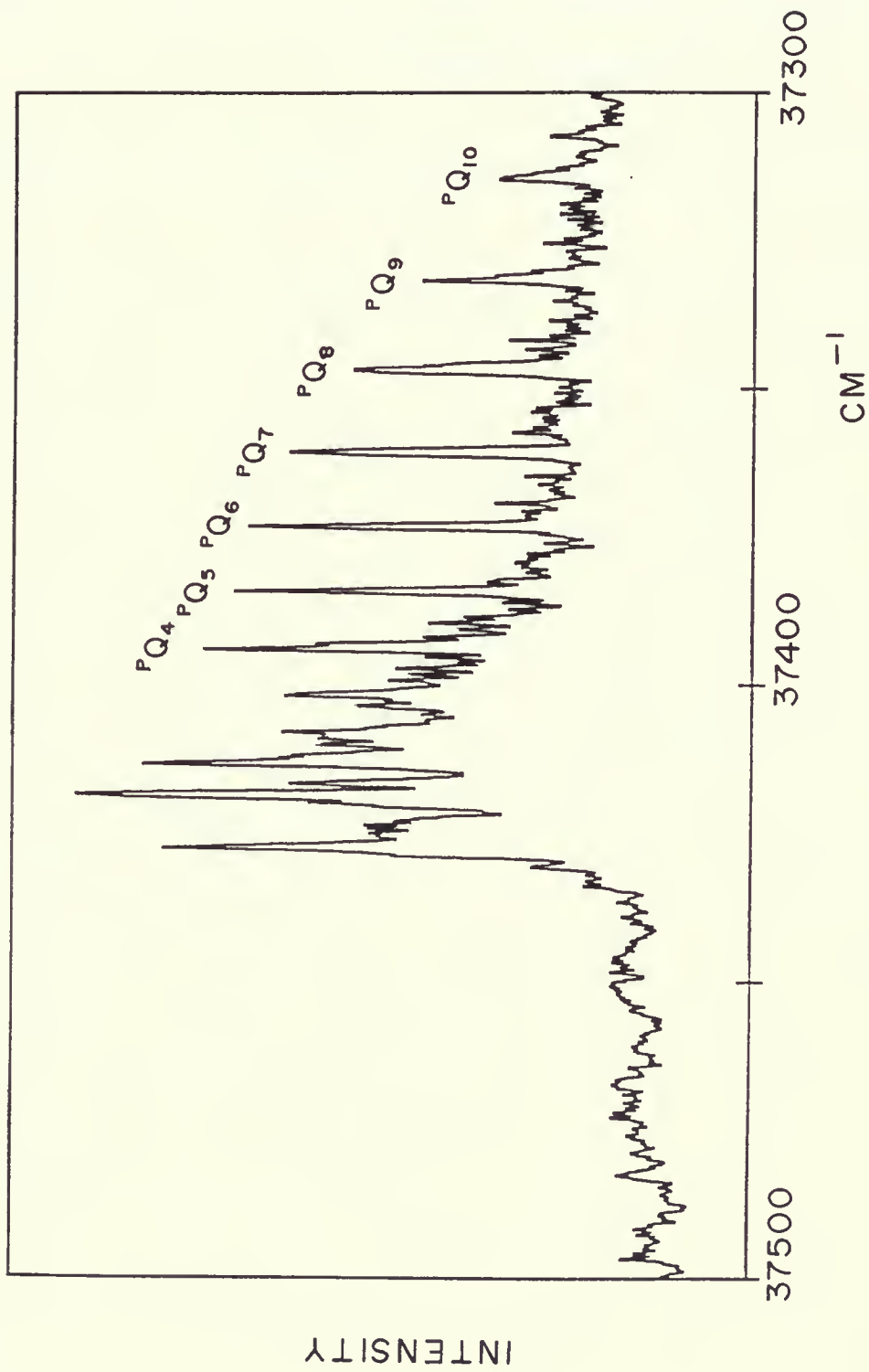




TABLE 8: OBSERVED  $P_{Q_k}$  SUBBAND HEADS IN THE ROTATIONAL SPECTRUM OF THE  
 $0^0_0$  BAND IN FORMIC ACID

K	$\text{cm}^{-1}$
4	37394.1
5	37384.3
6	37373.3
7	37360.8
8	37346.9
9	37331.8
10	37314.7

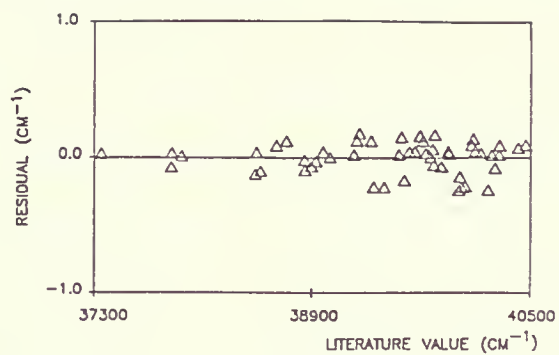




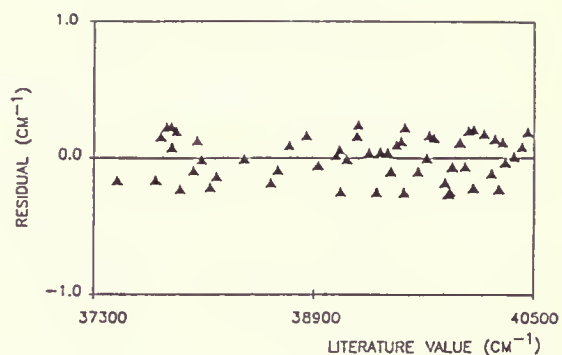
Figure 19  
Plots of the residuals versus literature values  
for the U/Ar lines identified for the  
calibration of the experimental spectra



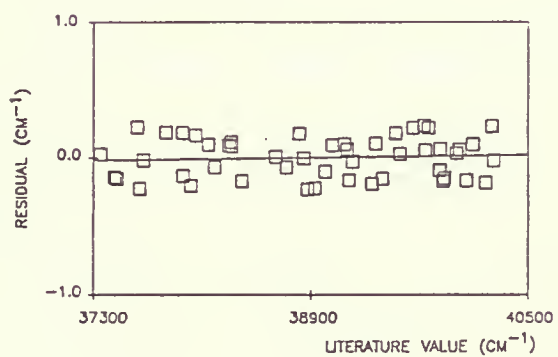
HCOOH



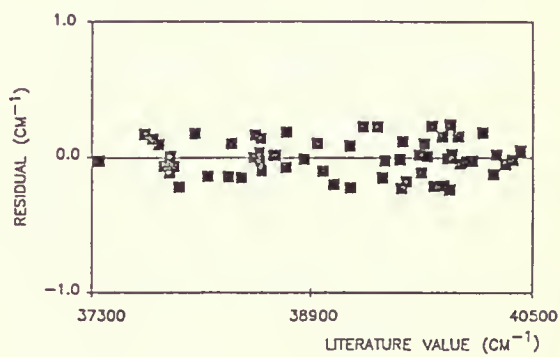
HCOOD



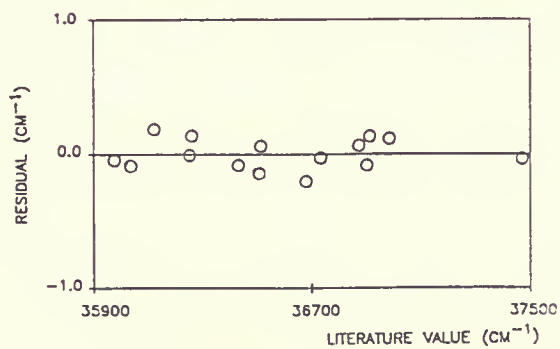
DCOOH



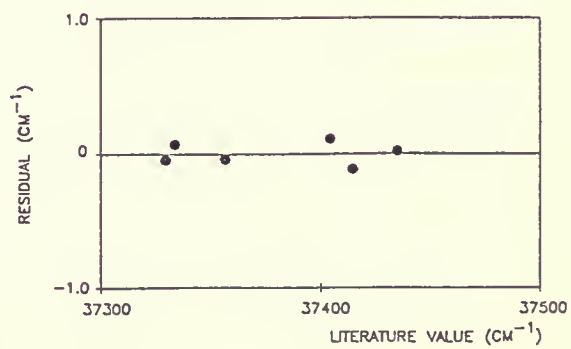
DCOOD



HCOOH



HCOOH





spectra involved locating the origin of this electronic transition.

In the 37000-40500  $\text{cm}^{-1}$  spectrum of  $\text{HCOOH}$  (Figure 13), the band at 37431.5  $\text{cm}^{-1}$  undergoes a +30.0  $\text{cm}^{-1}$  blue shift to 37461.5  $\text{cm}^{-1}$  in the spectrum of  $\text{HCOOD}$  (Figure 14). From this isotope shift, these vibrational bands are assigned as the respective electronic origins of the  $S_1 \leftarrow S_0$  transition. A similar +14.0  $\text{cm}^{-1}$  isotope shift is observed for the first band in  $\text{DCOOH}$  (Figure 15) and this is further shifted to +47.8  $\text{cm}^{-1}$  in  $\text{DCOOD}$  (Figure 16). The magnitude of the 14.0  $\text{cm}^{-1}$  aldehyde hydrogen isotope shift is expected and must be the consequence of the small amplitude but high frequency wagging mode,  $\nu_8=1033 \text{ cm}^{-1}$  in the  $S_0$  state converting into a large amplitude inversion motion in the upper  $S_1$  state. This effect is evident for the  $\text{CHOF}/\text{CDOF}$  pair of isotopomers where the origin isotope shift is observed to be 16  $\text{cm}^{-1}$ .<sup>54</sup> The source of the large isotope effect which is observed when the OH hydrogen is deuterated must be derived from a complimentary effect; namely, the  $\nu_9=642 \text{ cm}^{-1}$  torsional mode in the ground state converts into a large amplitude mode of low frequency as a result of a nonplanar distortion of the hydroxide hydrogen atom. On the basis then of the origin isotope effect, double quanta of the antisymmetric mode  $Q_8$  and  $Q_9$  should be active in the UV spectrum as type C bands. The activity of these modes is due to the nonplanar distortions



which accompany the electronic excitation.

The second band in the HCOOH spectrum at  $+251.2\text{ cm}^{-1}$  has about three times the strength of the origin band. The corresponding interval of  $+208.5\text{ cm}^{-1}$  in HCOOD allows these bands to be assigned to the torsional mode  $9^1_0$  band. The third band which is located at  $378.7\text{ cm}^{-1}$  in HCOOH has similar structural features to the  $9^1_0$  band and is identified as  $9^2_0$ . This torsional mode is also active in the spectra of the other species. The other vibrational modes were found to be less active in the spectra; nevertheless, could be located as suborigins for the well defined torsional mode. For HCOOH, the  $Q_7(\text{O}-\text{C}=\text{O})$  in-plane bending mode was observed as a weak band at  $403.5\text{ cm}^{-1}$  and  $Q_3(\text{C}=\text{O})$  as a band at  $+1115.2\text{ cm}^{-1}$ . These modes were also assigned in the spectra of the other isotopomers. Lastly, the first quantum of  $Q_8$ , the CH aldehyde wagging mode, does not create a strong band in the spectrum of HCOOH. A comparison of the HCOOH and DCOOH spectra showed that a band at  $865.4\text{ cm}^{-1}$  in the hydrogen compound shifts to  $715.0\text{ cm}^{-1}$  in the spectrum of the deuterated species. This interval was assigned to the  $8^2_0$  transition. It correlated with the corresponding intervals in formyl fluoride<sup>54</sup> and formyl chloride<sup>52</sup> of 924 and  $752\text{ cm}^{-1}$ , respectively. This mode has also been identified in the HCOOD and DCOOD spectra. The progressions involving the modes  $\nu_3$ ,  $\nu_7$ ,  $\nu_8$  and  $\nu_9$  were assigned as far as possible in the spectra of the four





isotopomers of formic acid. The short wavelength end of the spectra, unlike the rest of the spectra of the formic acid isotopomers, is complex and assignments of these bands were not clear.

One difficulty with the assignments is the labelling of the wagging and torsional transitions. As the barrier for inversion by the  $\nu_8$  wagging motion is expected to be fairly high, the transitions to the lower member of the inversion doublet  $0^+$ , will result in a type C band ( $0_0^0$ ). On the other hand, transitions to the upper member  $0^-$ , give rise to a band of AB mixed polarization ( $8_0^1$ ) due to vibronic coupling (Section 2.1). The situation for  $\nu_9$ , the other out-of-plane vibration, is somewhat different. In the molecular orbital calculations which follow, the difference between the anti and syn conformer in the  $S_1$  excited electronic state is about  $338 \text{ cm}^{-1}$ . Since the first torsional level of the anti species of HCOOH is located at  $T_0 + 251.2 \text{ cm}^{-1}$ , a value below the equilibrium position of the syn isomer, it will not be accompanied by an inversion doublet. Consequently, the first torsional transition, which is observed at  $37682.7 \text{ cm}^{-1}$  in HCOOH is given the label  $9_0^1$  rather than  $9_0^2$ .

For HCOOH, the vibrational spectrum was extended to include the  $35900\text{--}37500 \text{ cm}^{-1}$  region (Figure 17). Unfortunately, only one band could be identified,  $0_0^0$ . Although other sharp bands appear, their assignment is not



definite. This  $0_0^0$  was also recorded at higher resolution to view the rotational fine structure in greater detail. At the high frequency end of the observed rovibronic spectrum, for low  $K$  and high  $J$  values, the subbands are congested and complex. At the other end of the spectrum; however, for low  $J$  and high  $K$  values, the subbands are distinct and well separated from each other. These were assigned to the  $PQ_K$  heads (Figure 18). The centre of the band was estimated to be at  $37418.0 \text{ cm}^{-1}$ . The spacing between these band heads decreases towards the high frequency end, indicating that the rotational constants for the upper electronic state are different from those of the lower electronic state. Spectra of A-type, B-type and C-type bands were computed and compared to the observed spectrum to determine the origin band type. These contours and the observed spectrum are shown in Figure 20. The observed band appears to be of mixed A, B and C polarization. The ratios have not been determined, but the contributions for the band types near the band centre are depicted in the observed  $0_0^0$  band (Figure 20) by hatched and solid lines. From this analysis, approximate values for the excited state rotational constants were determined:  $A'=1.8619$ ,  $B'=0.4073$  and  $C'=0.3387 \text{ cm}^{-1}$ .

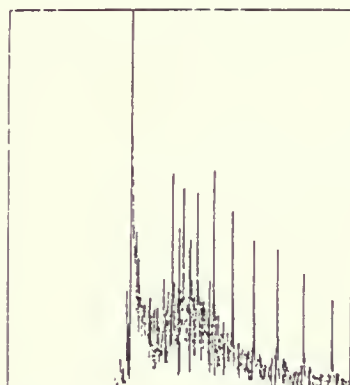


Figure 20  
Observed  $0^0_0$  band and the computed A-type,  
B-type and C-type bands

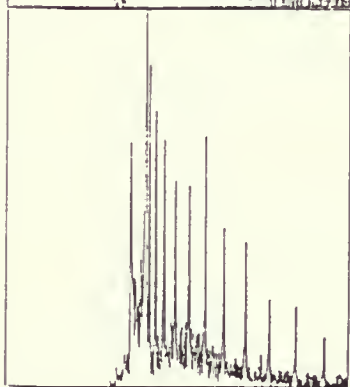
The hatched area denoted by /  
is for type A, solid line for  
type B and the hatched area  
denoted by \ is for type C  
contributions to the observed  
band



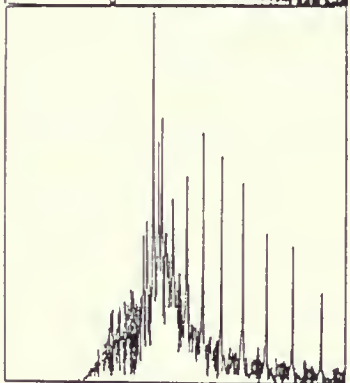
HCOOH



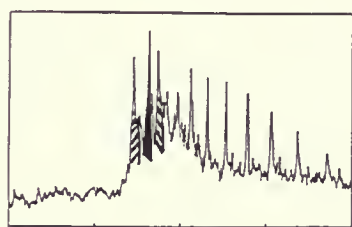
Type A



Type B



Type C



O-H Band

37500 37400 37300





## (II) Theoretical Calculations

Ab initio methods are powerful tools for determining the properties of molecular systems. In this study, the theoretical computations were carried out with the Gaussian 86 system of programs. The structure and dynamics of the formic acid monomer for the  $S_0$ ,  $T_1(n,\pi^*)$  triplet state and the corresponding  $S_1(n,\pi^*)$  state were evaluated. These calculations were undertaken to aid in the assignment of the observed UV spectrum.

The first excited singlet and triplet states of carbonyl molecules are derived from the electronic configuration  $(n)^1(\pi^*)^1$  and have similar properties. For example, in the case of the carbonyl prototype  $\text{CH}_2\text{O}$ , the  $S_1/T_1$  pair of states have structures which are nonplanar by 34.0/41.1 degrees and barrier heights to molecular inversion of 350.3/775.6  $\text{cm}^{-1}$ .<sup>87</sup> Likewise, the C=O bond lengths are similar, 1.323/1.307 Å. Initially, for the ease of computation the Hartree-Fock procedure was used to describe the  $S_0$  and  $T_1$  states. These findings were utilized in the interpretation of the excitation spectra as the  $S_1$  and  $T_1$  states are expected to have similar characteristics. This assumption was further reaffirmed when less extensive calculations with the GVB technique were carried out for the  $S_0$  and  $S_1$  states.

Tables 9 and 10 list the total energies and optimised molecular geometries obtained by the analytic energy gradient



TABLE 9: MOLECULAR STRUCTURE OF FORMIC ACID IN THE  $S_0$  GROUND  
AND  $T_1$  ELECTRONIC STATES<sup>a</sup>

	r(C=O)	r(CH)	r(CO)	r(OH)	$\alpha$ (COH)	$\alpha$ (OCH)	$\alpha$ (OCO)	$\theta$ (tor)	$\alpha$ (oop)
$S_0$ GROUND ELECTRONIC STATE									
A	1.1819	1.0835	1.3227	0.9533	108.71	124.74	124.87	0.0	0.0
B	1.1756	1.0900	1.3283	0.9481	111.52	123.17	122.98	180.0	0.0
C	1.1743	1.0873	1.3510	0.9504	111.76	122.98	123.96	95.11	0.0
$T_1$ EXCITED ELECTRONIC STATE									
D	1.3610	1.0780	1.3546	0.9489	110.31	-122.12	113.55	67.99	45.87
E	1.3556	1.0831	1.3526	0.9527	111.12	-118.50	113.00	-58.29	40.71
F	1.3588	1.0816	1.3571	0.9494	111.29	-120.52	113.25	-3.71	44.15
G	1.3574	1.0824	1.3550	0.9466	111.27	-119.55	111.11	-134.37	42.96
H	1.3562	1.0673	1.3451	0.9513	110.96	-118.89	115.93	80.93	1.09
I	1.3620	1.0632	1.3528	0.9482	110.80	-120.94	117.06	0.0	0.0
J	1.3558	1.0657	1.3521	0.9462	109.86	-119.51	113.41	180.0	0.0

a) in Å and degrees. See figure 22 for a description of the structures A-J.  
These calculations involved the HF approximation with a 6-31G\* basis set.



TABLE 10: TOTAL ENERGY OF FORMIC ACID IN THE  $S_0$  AND  $T_1$  ELECTRONIC STATES

Structure <sup>a</sup>	ENERGY (a.u.)	RELATIVE ENERGY ( $\text{cm}^{-1}$ )
$S_0$ GROUND ELECTRONIC STATE		
A	-188.762309667	0.000
B	-188.752546012	2142.873
C	-188.740660317	4751.482
$T_1$ EXCITED ELECTRONIC STATE		
D	-188.648594477	0.000
E	-188.646480077	464.057
F	-188.645367933	708.145
G	-188.644183452	968.108
H	-188.636110898	2739.826
I	-188.631125772	3833.936
J	-188.630330829	4008.405

a) see figure 22.



method within the Hartree-Fock approximation. The RHF procedure was used for the  $S_0$  state and the UHF method for the  $T_1$  state. A 6-31G\* basis set was used for each state. The  $S_0$  calculations for the geometries are a replicate of the results listed in Table 1 using the same level of SCF theory. For the fully optimised anti conformer, structure A, the SCF calculation yielded a total energy of -188.76230 Hartrees. This value is to be compared with a total energy of -189.35757 Hartrees obtained<sup>22</sup> using a larger basis set, MP3/6-311+G\*, corrected for electron correlation. The optimised syn conformer, structure B, calculated at -188.75254 Hartrees is 2142.9  $\text{cm}^{-1}$  higher in energy. This value is higher than the experimental anti-syn energy difference which was determined to be 1365  $\text{cm}^{-1}$ .

Vibrational frequencies were calculated by the analytical SCF second derivative technique. A comparison of the calculated and observed infrared frequencies for the anti rotamer, in Table 11, shows good agreement. The values obtained for the syn isomer display significant frequency shifts. For example,  $\nu_3(\text{C=O})$  anti is calculated to absorb at 1832  $\text{cm}^{-1}$  in the infrared, whereas the corresponding band in the syn species is predicted to be at 1872  $\text{cm}^{-1}$ . A description of the vibrational frequencies of the normal mode coordinates for anti and syn HCOOH in the ground state is given in Figure 21. The calculated frequencies for anti HCOOH





TABLE 11: VIBRATIONAL FREQUENCIES OF FORMIC ACID IN THE  $S_0$   
AND  $T_1$  ELECTRONIC STATES<sup>a</sup>

MODE	approx. descr.	GROUND STATE $\tilde{X}^1A'$			EXCITED TRIPLET STATE $\tilde{a}^3A$		
		anti	expt. <sup>b</sup>	syn	anti	expt. <sup>d</sup>	syn
$\nu_1$	(O-H)	3638	3569	3696	3678	--	3604
$\nu_2$	(C-H)	2988	2942	2905	2996	--	2936
$\nu_3$	(C=O)	1832	1777	1872	1132	1115	1154
$\nu_4$	(H-C-O)	1397	1381	1425	1356	--	1317
$\nu_5$	(H-O-C)	1296	1223 <sup>c</sup>	1283	1234	--	1251
$\nu_6$	(C-O)	1148	1104	1113	1073	--	1063
$\nu_7$	(O-C=O)	623	625	652	430	404	458
$\nu_8$	(H-C oop)	1073	1033	1062	910	865	896
$\nu_9$	(H-O oop)	644	642	466	272	251	224

a) in  $\text{cm}^{-1}$ , scaled values = calculated x 0.9.

b) Ref. 31

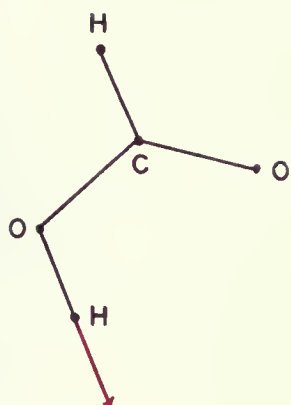
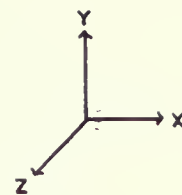
c) Ref. 19. The reported vibrational frequencies of  $\nu_3$  and  $\nu_7$  for the syn isomer are 1744.7 and 1124.2  $\text{cm}^{-1}$ , respectively.

d) values obtained from  $S_1 \leftarrow S_0$  electronic transition.

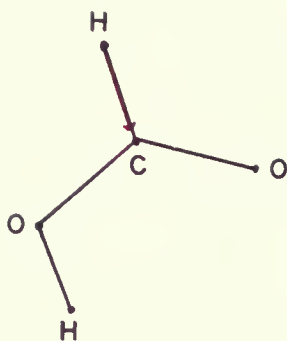


Figure 21  
Description of the vibrational frequencies of the  
normal mode coordinates for Anti and Syn HCOOH,  
respectively in the  $S_0$  state

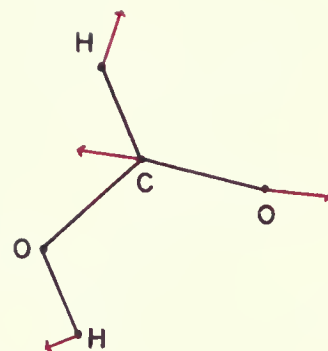




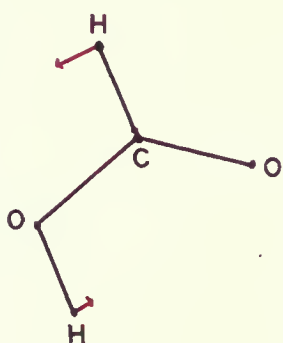
$\nu_1$  (3638)



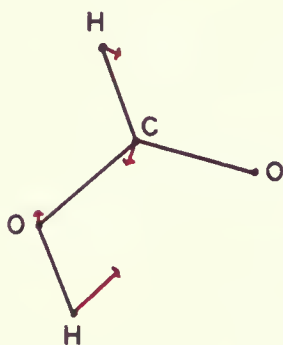
$\nu_2$  (2988)



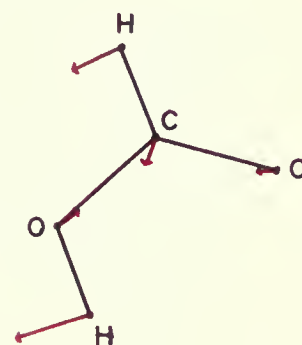
$\nu_3$  (1832)



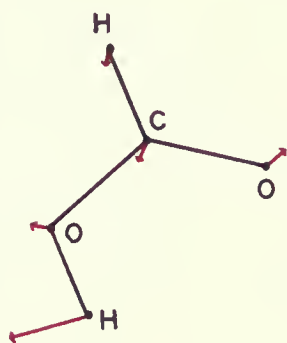
$\nu_4$  (1397)



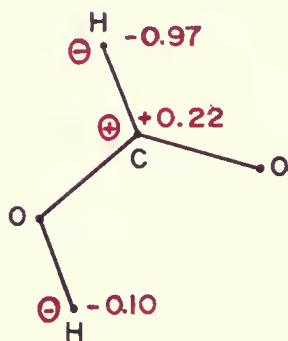
$\nu_5$  (1296)



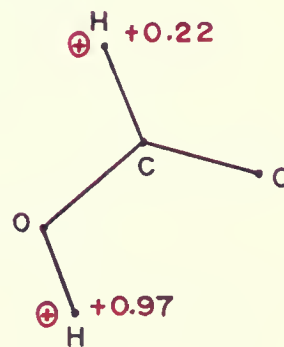
$\nu_6$  (1148)



$\nu_7$  (623)

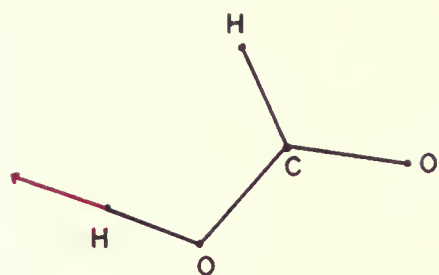
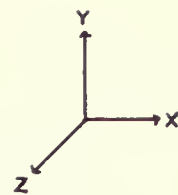


$\nu_8$  (1073)

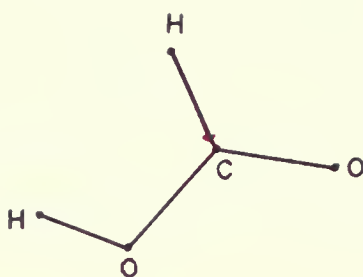


$\nu_9$  (644)

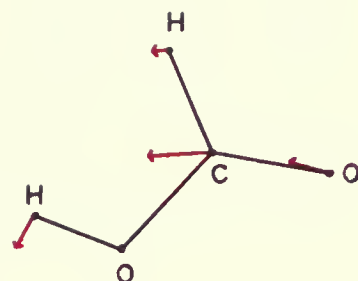




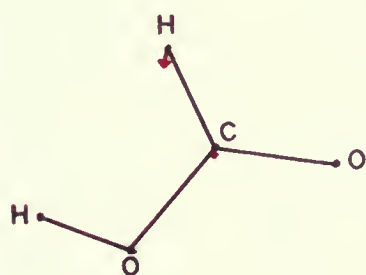
$\nu_1$  (3696)



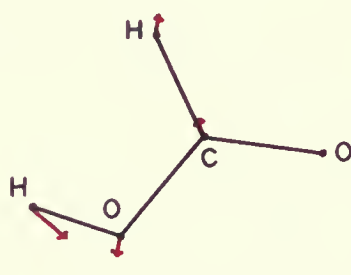
$\nu_2$  (2905)



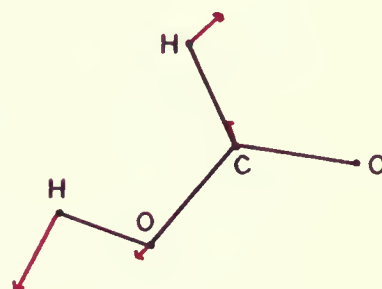
$\nu_3$  (1872)



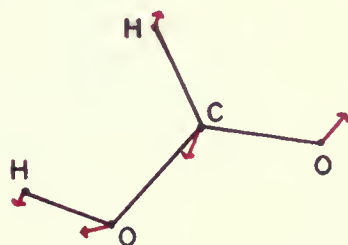
$\nu_4$  (1425)



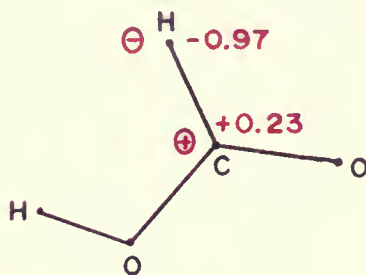
$\nu_5$  (1283)



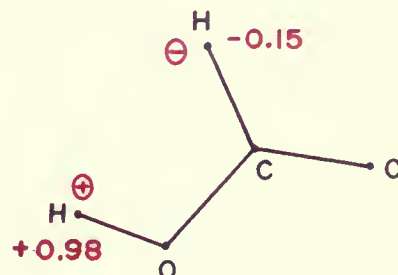
$\nu_6$  (1113)



$\nu_7$  (652)



$\nu_8$  (1062)



$\nu_9$  (466)





resemble those obtained using a DZ+P basis set (Table 2) for the monomer. The first four frequencies,  $\nu_1, \dots, \nu_4$ , may be considered to be valence vibrations; that is, their vibrational motion is localized in one or two bonds in the molecule. The remaining vibrations are due to skeletal motions; thus, the labels to these normal coordinates are only approximate.

The description of the excited state structure and dynamics is more complex. The optimization procedure revealed a number of minima, maxima and saddle points in the vibrational potential. The total energies, bond lengths and bond angles for these structures are given in Tables 9 and 10. A minimum in the  $T_1$  energy was found for structure D. The geometry of this equilibrium conformer of formic acid is somewhat unusual, in that the torsional and wagging angles, 67.99 and 45.87 degrees, respectively, are directed out of the opposite sides of the O-C=O molecular plane, in an anti configuration. A second structure D\* which is isoenergetic with D, is obtained by inverting the torsional and wagging angles to -67.99 and -45.87 degrees. These points can be represented by Newman projection diagrams on a potential surface which is given in Figure 22. Structure I, at 3833.9  $\text{cm}^{-1}$  above D, has both OH and CH groups in the plane of the molecule. It lies at a position of maximum potential energy and may be regarded as the transition state for the D-D\*

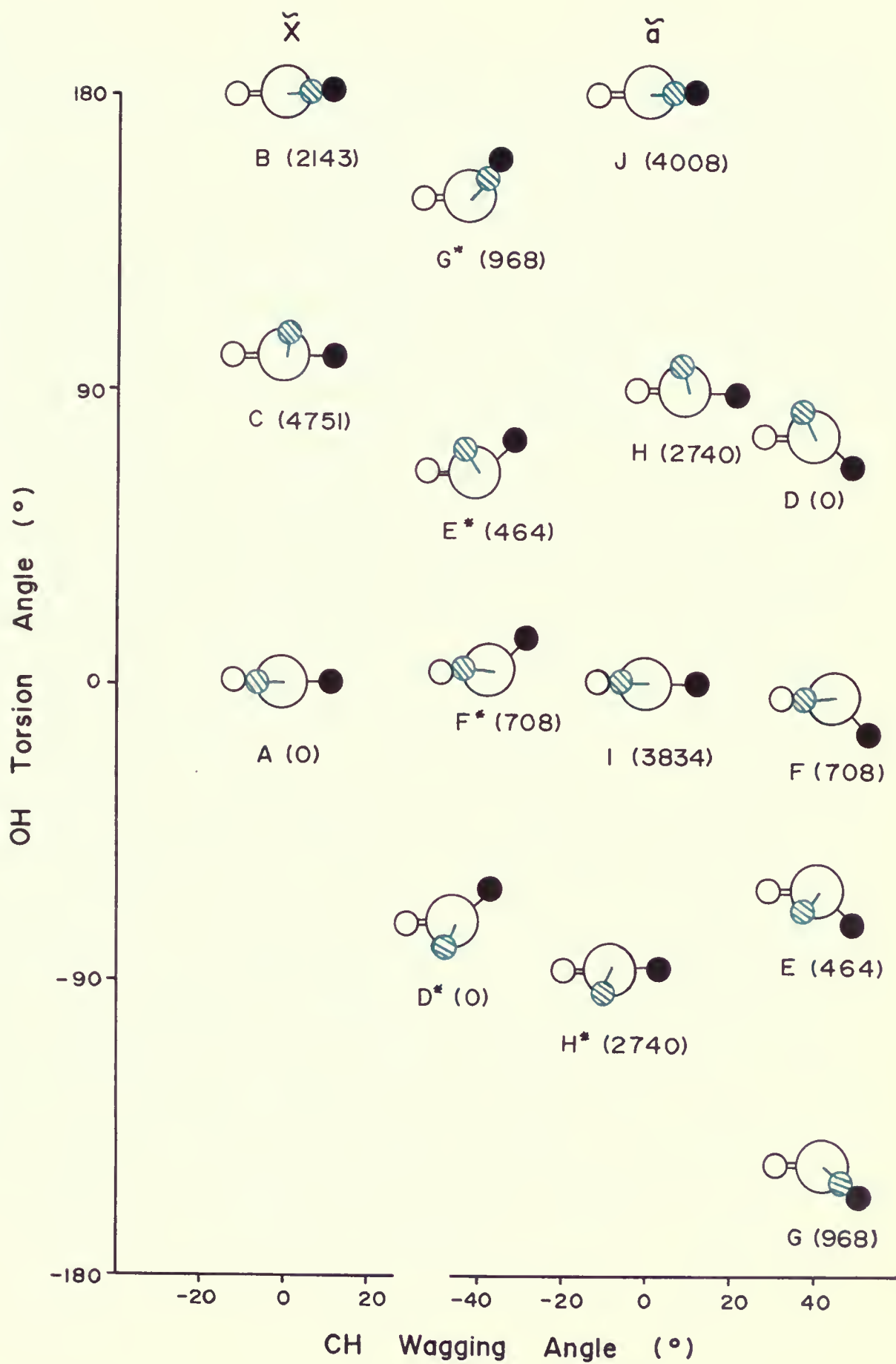


Figure 22

Newman projection diagrams illustrating the Molecular  
structure of formic acid in the ground  
 $S_0$  and  $T_1$  excited electronic states

The horizontal axis is defined by the O-C=O molecular plane with the CH and OH hydrogens denoted as solid and hatched circles, respectively. The carbonyl oxygen is drawn as an open circle. The bracketed values are the optimised energy points in  $\text{cm}^{-1}$  relative to the equilibrium positions which are scaled to 0  $\text{cm}^{-1}$ . The asterisks refer to structures which are related by the nonrigid switch operation.







inversion process. The second stable conformer, E, lies 464.1  $\text{cm}^{-1}$  above D and has the torsional and wagging hydrogens directed on the same side of the O-C=O frame by -58.29 and 40.71 degrees. Inversion of this structure through I leads to the isoenergetic structure E\*. Saddle points F, G, and H, with one unbound coordinate, were calculated to have energies of 708.1, 968.1 and 2739.8  $\text{cm}^{-1}$ . The least stable position of maxima, J, corresponds to a syn planar configuration and is 4008.4  $\text{cm}^{-1}$  above D.

The vibrational frequencies calculated for the  $T_1$  structure D are collected together in Table 11 along with the observed  $S_1$  frequency intervals. The agreement for the  $\nu_3(\text{C=O})$  stretching mode (calc=1132, obs=1115  $\text{cm}^{-1}$ ) is surprisingly good, as the level of calculations considered here tends to overestimate the C=O bond length for the  $T_1$  states. The frequency for the wagging mode,  $\nu_8(\text{H-C oop})$  is calculated to be 910  $\text{cm}^{-1}$  in agreement with the observed interval of 865  $\text{cm}^{-1}$ . This is not unreasonable, since the barrier to inversion along the path D-I-D\* is high, 3834  $\text{cm}^{-1}$ . In this case, the bottom of the well would be governed by a potential which is largely quadratic and would allow the vibrational frequencies to be calculated in the harmonic approximation. The observed activity in the  $\nu_7(\text{O-C=O})$  bending mode is not unexpected, since the frequency in the two states is quite different ( $S_0/T_1=623/430$   $\text{cm}^{-1}$ ). Moreover, the





calculated O-C=O angle in the  $S_0/T_1$  states is 124.87/113.55 degrees (HF approximation). This reduction in bond angle in the excited state leads to a larger rotational constant about the a principal axis, resulting in the open K-type rotational structure evident in the spectra. The vibrational frequencies for the  $\nu_9$ (H-O oop) mode in the  $S_0/T_1$  states are 644/272  $\text{cm}^{-1}$ . This is a consequence of the differing barriers to anti-syn conversion. The out-of-plane displacement is described by a large amplitude twisting motion of low frequency which contributes to the flexibility of the molecule in the excited state. The displacements for the normal vibrations of formic acid are given in Tables 12 and 13. Unlike the ground state, these frequencies all have contributions in the x, y, z directions, making their description difficult.

Lastly, the results from the GVB technique utilizing the 6-31G\* basis set will be discussed. The  $S_0$  and  $S_1$  equilibrium structures are reported in Table 14 and the corresponding energies are given Table 15. Photographic depictions of the anti and syn conformers in these two states are shown in Figure 23. These diagrams were made by inputting the x, y, and z values derived from the computations for each of the geometries into a program called Alchemy for the IBM computer. The values for the bonds lengths and angles in this calculation for the  $S_0$  state are similar to those obtained using the HF approximation (Table 9). Thus, the two methods



TABLE 12: DISPLACEMENTS FOR THE NORMAL VIBRATIONS OF ANTI FORMIC ACID<sup>a</sup> IN THE T<sub>1</sub> STATE

	C	O(C=O)	H(C-H)	O(C-O)	H(O-H)
$\nu_1$	(x) 0.00128 (y) 0.04601 (z) -0.03741	-0.02385 -0.03020 0.02665	-0.03565 -0.01661 -0.17978	-0.00837 0.03423 0.04837	0.53169 -0.59532 -0.56546
$\nu_2$	-0.02433 -0.32770 -0.10780	0.40168 0.11994 0.05237	0.08918 -0.41330 -0.26836	-0.36466 0.16223 0.06641	-0.38701 -0.16312 -0.33323
$\nu_3$	-0.02486 -0.04163 -0.13726	0.05447 -0.04801 0.03038	-0.03164 0.44412 0.79803	-0.05375 -0.01362 0.01090	0.31622 0.03838 0.18125
$\nu_4$	-0.14365 0.26290 0.14432	0.21189 -0.17906 -0.05503	-0.78649 0.12445 -0.30693	-0.03738 -0.02594 -0.02997	-0.27258 -0.00115 -0.06248
$\nu_5$	-0.19173 -0.16398 -0.13333	-0.01026 -0.00277 0.02174	-0.79109 -0.00840 0.17258	0.22713 0.12393 0.08191	-0.36789 0.02109 -0.22995
$\nu_6$	0.19232 0.05528 -0.06077	-0.04142 0.01490 0.02232	-0.28996 0.20703 0.17310	-0.03611 -0.05516 0.03660	-0.76951 -0.22632 -0.38456
$\nu_7$	0.14155 -0.06760 0.03089	-0.03383 0.01408 0.01619	-0.81884 -0.03960 -0.08798	-0.04902 0.02949 -0.04960	0.44842 0.15308 0.25054
$\nu_8$	0.00787 0.07724 -0.03130	-0.00030 0.00042 -0.00087	-0.07593 -0.91036 0.39784	-0.00061 -0.00157 -0.00009	-0.00335 0.00884 -0.00999
$\nu_9$	-0.00070 0.00069 -0.00132	-0.00027 0.00023 0.00000	-0.00095 -0.01145 0.00508	0.01226 0.04785 -0.03846	-0.18104 -0.75986 0.62109

a) anti refers to structure D in Figure 22.



TABLE 13: DISPLACEMENTS FOR THE NORMAL VIBRATIONS OF SYN FORMIC ACID<sup>a</sup> IN  
THE T<sub>1</sub> STATE

	C	O(C=O)	H(C-H)	O(C-O)	H(O-H)
$\nu_1$	(x) 0.00666 (y) -0.01692 (z) 0.06042	-0.02866 0.01390 -0.03812	0.02582 -0.07025 0.13438	-0.01045 -0.04347 -0.04019	0.51559 0.74100 0.38905
$\nu_2$	-0.02892 0.36392 0.01041	0.42678 -0.13259 -0.01613	0.10248 0.32022 0.09666	-0.38319 -0.17883 -0.01551	-0.44991 0.28903 0.28150
$\nu_3$	0.01850 0.00146 0.13891	-0.01516 -0.02302 -0.03962	0.03304 0.57189 -0.70112	-0.02165 -0.00402 -0.01361	0.33082 -0.16009 -0.15092
$\nu_4$	0.07383 0.32142 -0.00720	-0.22353 -0.19765 0.01077	0.60471 0.30209 0.08274	0.16025 -0.07381 -0.02388	-0.47959 0.17902 0.21096
$\nu_5$	0.25818 -0.12161 -0.01994	-0.05243 -0.05028 -0.00339	0.90717 -0.11989 0.05218	-0.19316 0.14441 0.01781	-0.08354 0.07384 -0.04357
$\nu_6$	-0.02462 0.09547 -0.10314	-0.01809 -0.02572 0.01061	0.17131 -0.09589 0.21467	-0.02735 -0.01840 0.06885	0.84305 -0.34058 -0.24772
$\nu_7$	0.23271 0.06101 -0.01799	-0.06338 -0.03475 0.02515	-0.95890 -0.07307 0.02508	-0.05515 -0.00455 -0.01068	0.06920 -0.02959 -0.04048
$\nu_8$	0.00666 -0.06925 -0.04444	-0.00044 -0.00049 -0.00122	-0.07103 0.82033 0.56141	0.00002 0.00076 -0.00106	-0.00168 -0.00008 0.00381
$\nu_9$	0.00003 0.00089 -0.00102	0.00004 -0.00016 0.00008	0.00287 -0.00469 -0.00016	-0.00685 0.03311 -0.05223	0.10496 -0.52881 0.83990

a) syn refers to structure E in Figure 22.



TABLE 14: CALCULATED MOLECULAR STRUCTURE OF FORMIC ACID IN THE  $S_0$  GROUND  
AND  $S_1$  ELECTRONIC STATES<sup>a</sup>

	r(C=O)	r(CH)	r(CO)	r(OH)	$\alpha$ (COH)	$\alpha$ (OCH)	$\alpha$ (OCO)	$\theta$ (tor)	$\alpha$ (oop)
$S_0$ GROUND ELECTRONIC STATE									
a	1.1824	1.0840	1.3234	0.9535	108.63	124.69	125.06	0.0	0.0
b	1.1761	1.0912	1.3287	0.9484	111.50	123.47	122.93	180.0	0.0
$S_1$ EXCITED ELECTRONIC STATE									
d	1.3743	1.0771	1.3515	0.9492	110.42	-122.63	112.87	63.66	45.76
e	1.3701	1.0821	1.3499	0.9524	110.71	-118.72	112.35	-47.91	41.32

a) in Å and degrees. See figure 23 for a description of the above structures.  
These calculations involved the GVB approximation with a 6-31G\* basis set.





TABLE 15: CALCULATED TOTAL ENERGY OF FORMIC ACID IN THE  $S_0$  AND  
 $S_1$  ELECTRONIC STATES

Structure <sup>a</sup>	ENERGY (a.u.)	RELATIVE ENERGY ( $\text{cm}^{-1}$ )
$S_0$ GROUND ELECTRONIC STATE		
a	-188.7747569936	0.000
b	-188.7648402037	2174.995
$S_1$ EXCITED ELECTRONIC STATE		
d	-188.6336441178	0.000
e	-188.6321054319	337.991

a) see figure 23.



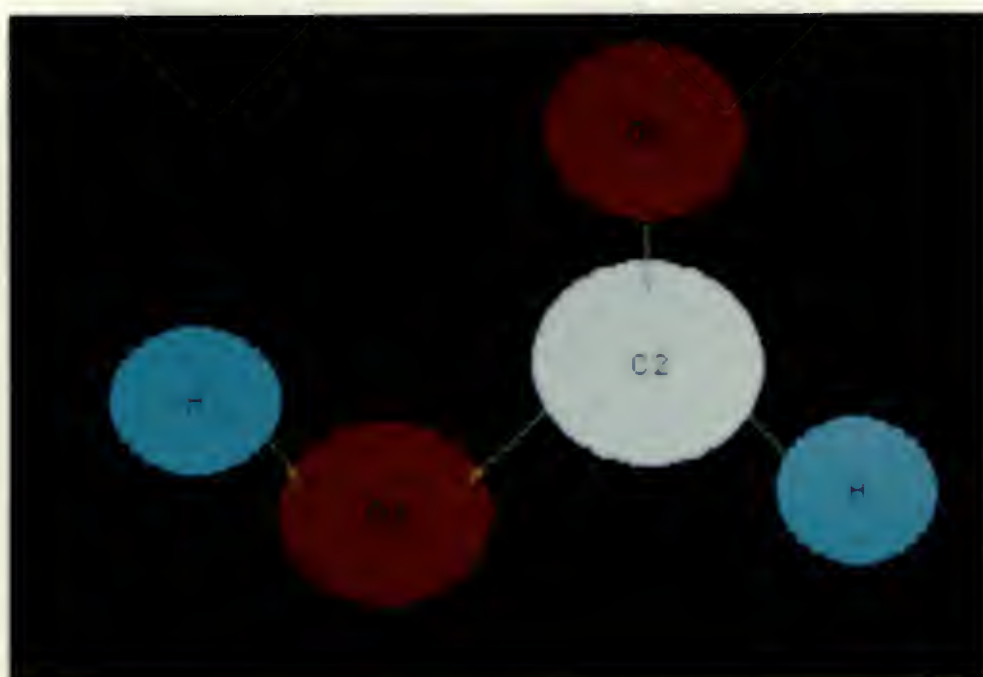
Figure 23

Photographs of the calculated ground state and singlet excited state geometries of Anti and Syn formic acid, respectively

- A) Top photograph displays the planar  $S_0$  form.
- B) Bottom photograph depicts the nonplanar  $S_1$  species. For the nonplanar case, the diagram is shown looking along the C-O bond.



(A)

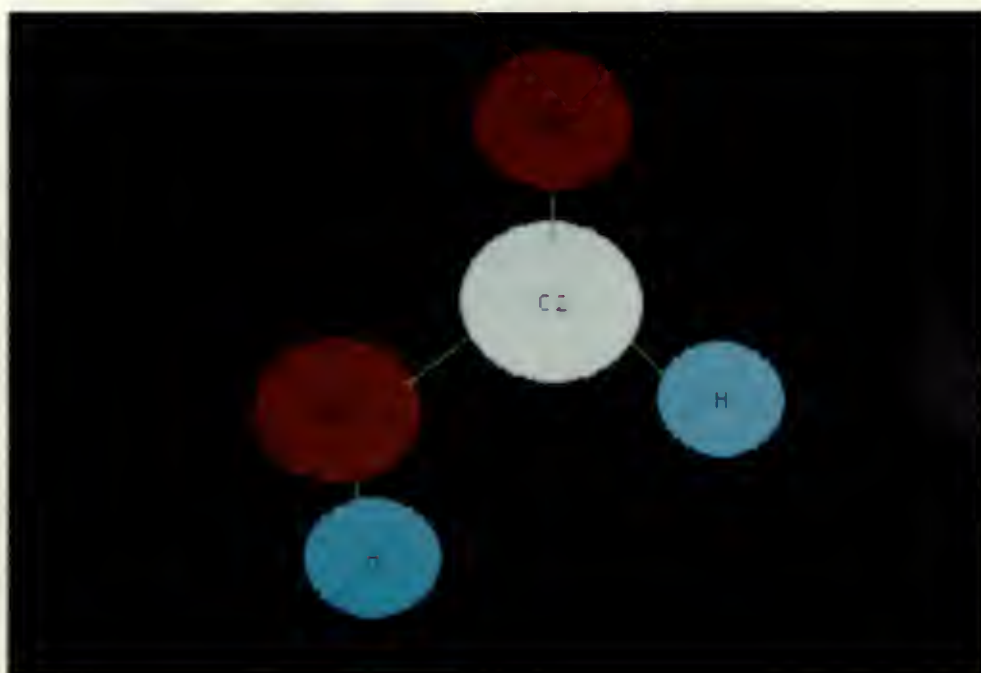


(B)

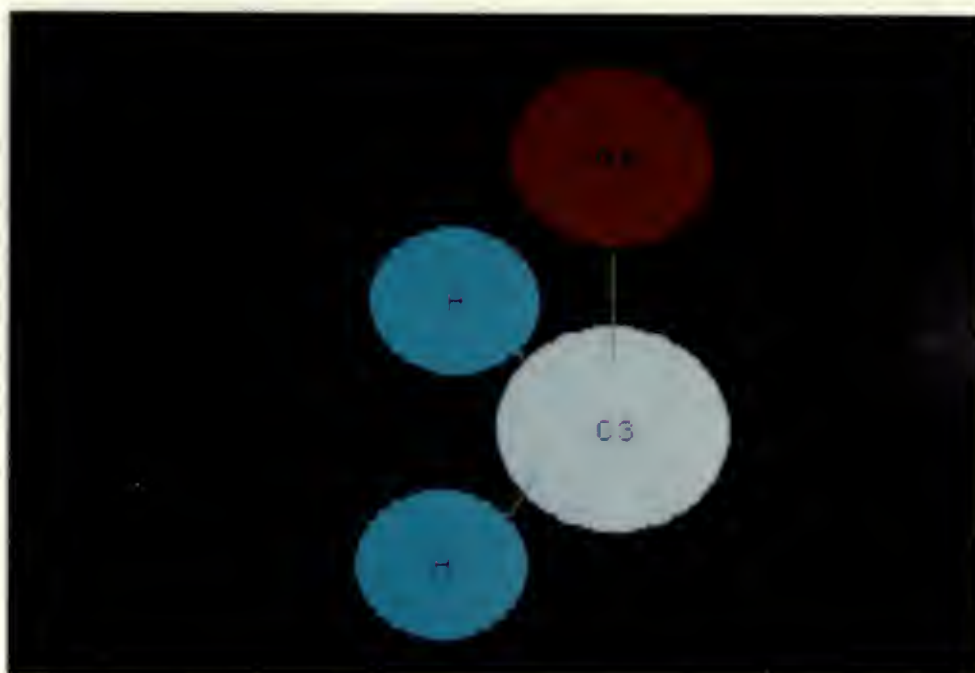




**(A)**



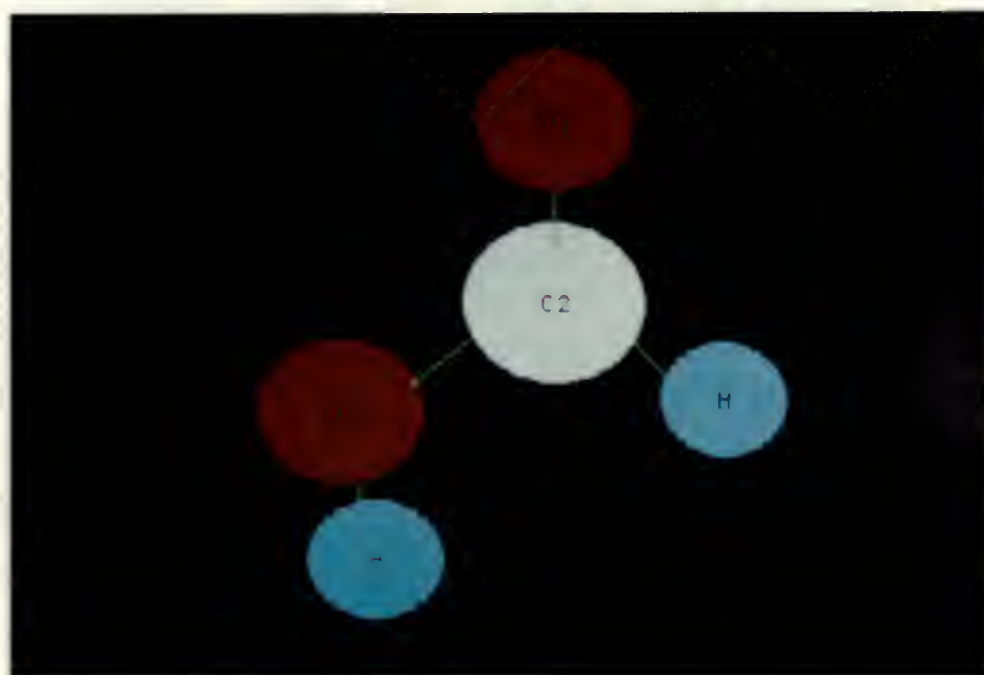
**(B)**



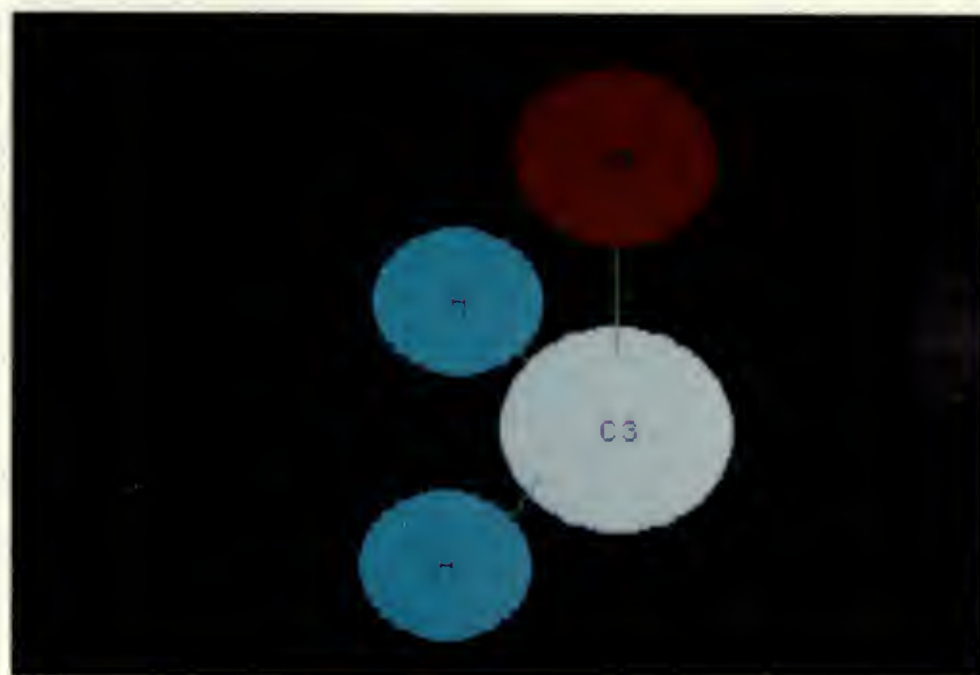




(A)



(B)





are complementary. In the ground state, the anti-syn difference is calculated to be  $2175\text{ cm}^{-1}$  with the anti conformer at lower energy. In comparison to the HF results; however, the energy of the anti species is approximately  $2730\text{ cm}^{-1}$  below the HF energy, a substantial improvement to the total energy.

The  $S_1$  and  $T_1$  results are also quite similar. The most marked differences appear in the C=O bond length and the torsional angles. For the  $S_1$  calculation, the C=O bond length increases in the  $S_1$  state:  $S_1/T_1$  is  $1.3743/1.3610\text{ \AA}$  for the anti conformer and  $1.3701/1.3556\text{ \AA}$  for the syn species. The OH torsional angles in  $S_1/T_1$  values are  $67.99/63.66$  degrees for anti and  $-58.29/-47.91$  degrees for syn formic acid.

In the  $S_1$  excited state the two conformers are separated by  $338\text{ cm}^{-1}$ , a value slightly smaller than the  $464\text{ cm}^{-1}$  determined for the HF calculation. Using the GVB calculated results, the excited singlet state is located at  $30\,971\text{ cm}^{-1}$  above the  $S_0$  ground state. The equilibrium rotational constants and dipole moments for the  $S_0$  and  $S_1$  states are given in Table 16. For the ground state, these values are in agreement with the experimental findings (Table 2). For the  $S_1$  state, the  $A_e$  rotational constant decreases significantly from the  $S_0$  value in accordance with the experimental rotational contour results. The total dipole moment for the anti and syn species in this  $S_1$  state are analogous at



TABLE 16: CALCULATED EQUILIBRIUM ROTATIONAL CONSTANTS AND DIPOLE  
MOMENTS FOR THE  $S_0$  AND  $S_1$  STATES

	$S_0$		$S_1$	
	anti	syn	anti	syn
A	80.0315	90.7916	60.4056	59.2147
B	12.4184	11.9913	11.1626	11.7841
C	10.7503	10.5923	10.0618	10.1769
$\mu^{\circ}$	1.57	4.34	1.19	1.76

a) rotational constants in GHz; dipole moments in Debyes. These calculations involved the GVB approximation with a 6-31G\* basis set.



1.186/1.757 Debyes, respectively, different from the  $S_0$  findings. In summary then, for the calculations involving the  $S_1$  state, it is clear that the properties of the  $S_1$  and  $T_1$  states are similar; justifying the use of the  $T_1$  calculated data in the assignment of the observed  $S_1$  spectrum.





## CHAPTER 6

## REMARKS AND CONCLUSIONS

The vapour phase absorption spectrum of formic acid which arises from an  $n \rightarrow \pi^*$  electron promotion consists of a complex of bands which are built onto the side of a strong absorption continuum. The fluorescence excitation spectrum of formic acid in this region is greatly simplified and consists of a group of bands which display a well defined rotational fine structure. A comparison of the deuterium-hydrogen frequency shifts among the four isotopomers of formic acid allowed the origin to be assigned to the band at  $37431.5 \text{ cm}^{-1}$ . The modes  $\nu_3(\text{C=O})$ ,  $\nu_7(\text{O-C=O})$ ,  $\nu_8(\text{CH})$  and  $\nu_9(\text{OH})$  were observed to form intervals in the spectrum. The activity of the  $\nu_9$  torsional mode in the vibrational spectrum is of particular interest; it results from an  $S_1$  equilibrium configuration where the OH group is twisted from the O-C=O frame of the molecule. The activity of the  $\nu_8$  mode demonstrates that the CH bond is also displaced from the molecular plane. Both the aldehyde and the hydroxy groups would be distorted from the O-C=O molecular frame, which would result in a complex equilibrium structure for  $S_1$  formic acid.

The rotational analysis of the  $0_0^0$  band of formic acid showed that this band is a hybrid composite built from A, B and C type bands. The rotational origin is predicted to be at  $37418.0 \text{ cm}^{-1}$ ; however, the polarization of this band was



not determined as the resolution of the rotational structure was not adequate to obtain a definitive rotational assignment. Thus, the splitting for the  $0^+-0^-$  levels and consequently the barrier height to inversion of the formyl hydrogen was not determined. Nevertheless, the rotational band contour analysis showed that the greatest change in the rotational constant is for the  $A''/A'$  pair:  $2.5855/1.8619\text{ cm}^{-1}$ . From the estimated rotational constants for the excited state the inertial defect is calculated to be approximately  $-5.8\text{ amu \AA}^2$ . The magnitude and sign of this value once again confirms the nonplanar nature of the molecule in the excited state. Although the excited state parameters were not derived rigorously, the important changes in the molecule are in the C=O bond length, the OCO angle and the nonplanarity due to the formyl and hydroxyl hydrogens.

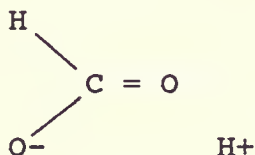
The equilibrium structure and the dynamics of the  $S_0$ ,  $T_1$  and  $S_1$  states of formic acid were evaluated by ab initio SCF theory using a 6-31G\* basis set. The calculations correctly showed that the anti was more stable than the syn conformer in the lower electronic state, although the calculated  $2140/2180\text{ cm}^{-1}$  energy differences for the HF/GVB pair were substantially larger than the experimental value of  $1365\text{ cm}^{-1}$ . The structures calculated for the  $S_1$  and  $T_1$  states were more complex, but similar. For the  $S_1$  state the stable equilibrium configuration was calculated to have the OH and CH bonds



twisted from the O-C=O frame by 63.66 and 45.86 degrees, respectively. The calculations predicted a second conformation with torsional and wagging angles of -47.91 and 41.32 degrees. This form is less stable by 338  $\text{cm}^{-1}$ .

The geometry of formic acid changes considerably in the  $S_1$  excited electronic state. The ab initio calculations show that the C=O bond length increases while the O-C=O angle decreases upon excitation for the anti species. A similar trend is observed for the syn conformer. The formyl and hydroxyl hydrogens also contribute to the unusual structure of the molecule as they adopt out-of-plane behaviour. As in the ground state, two conformers are possible; however, in this case the barrier height to anti-syn conversion is lower,  $S_0/S_1 \approx 2100/350 \text{ cm}^{-1}$  with the anti species being the most stable form for both states.

For the ground state, the different bonding effects in the anti and syn isomers result in small structural differences in the calculated angles and bond lengths. The contribution of the resonance structure





is expected to stabilize the anti isomer as a result of the electrostatic attraction between the H<sup>+</sup> and O<sup>-</sup> atoms. The shortening of the C=O and the lengthening of the C-O bonds of -0.006 and +0.007 Å, respectively for the anti relative to the syn species may be attributed to this effect. On the other hand, for the S<sub>1</sub> state, the wagging and torsion in the molecule leads to complexity as the CH and OH groups are distorted from the molecular frame. The anti species is still the predominant isomer; however, as the energy values for the two forms are not so different the electrostatic effect is not as significant. The total dipole moment calculations also support these findings;  $\mu_{\text{anti}}/\mu_{\text{syn}}$  is 1.579/4.346 for the S<sub>0</sub> state and 1.186/1.757 Debyes for the S<sub>1</sub> state. The question still remains, why does the molecule have such an unusual structure in the lowest lying excited state?

Insight into the structural question posed can be drawn from the molecular orbital calculations. For the n $\rightarrow\pi^*$  electronic excitation, an electron from the n nonbonding orbital on the oxygen carbonyl chromophore is promoted to an antibonding orbital,  $\pi^*$ . Figure 2 describes this transition with the use of localized MO's; however, for formic acid this simplistic model is not appropriate. The GVB calculations on the S<sub>0</sub> state show that the hydroxyl oxygen plays a role in the formation of the antisymmetric molecular orbitals. The molecular orbitals of interest are those involving  $\pi_{\text{C=O}}$ ,





$n_{\text{O(OH)}}$  and the  $\pi^*_{\text{(C=O)}}$ ,  $n_{\text{O(OH)}}$  which are depicted in Figure 24 for the anti species. The coefficient values for the atomic orbitals are similar for anti and syn with a change of sign on the atomic orbitals for the molecular orbital labelled 2a" (Figure 4). The molecular orbital labelled 3a" is unoccupied in the ground state and orbital 10a' which has a large electron density localized on the nonbonding oxygen of the carbonyl group is not shown.

Due to the electron promotion, the molecule tends to rearrange its structure to decrease the antibonding character and to achieve stability by diminishing the energy in the system. Contributions from the  $p_z$  atomic orbitals on the OH oxygen cannot be neglected in the discussion as the antibonding character across the C-O bond is evident in the orbital labelled 3a", and not only across the C=O bond. Using Walsh's rules<sup>75</sup> the energy in a system can be decreased if an antibonding p atomic orbital is converted to an s atomic orbital. In formic acid, this can be accomplished by distorting the molecule from a planar to nonplanar configuration at the carbon centre. As the molecule distorts from the plane, the  $\pi^*$  orbital changes from a p atomic orbital on the carbon centre to an  $sp^3$  hybrid orbital. At the other end of the molecule, a similar out-of-plane behaviour is observed. Figure 24 shows that the nonbonding out-of-plane oxygen orbital becomes antibonding with respect to the

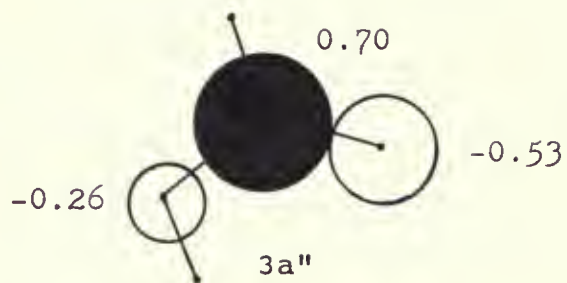
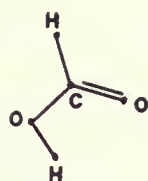


Figure 24

Description of the antisymmetric  $p_z$  molecular  
orbitals of anti formic acid

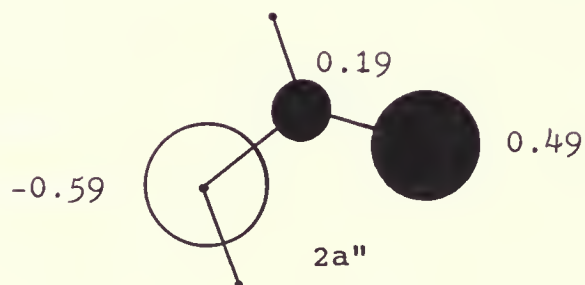
Filled and open circles are used to  
denote the sign of the lobe in view as  
descriped by the MO coefficients



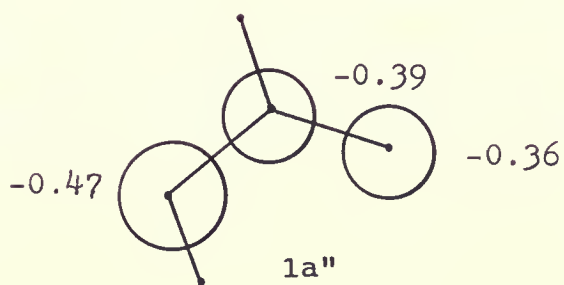


$\pi^*_{(\text{C}=\text{O})}, n_{\text{O}(\text{OH})}$

E ↑



$\pi_{(\text{C}=\text{O})}, n_{\text{O}(\text{OH})}$



$\pi_{(\text{C}=\text{O})}, n_{\text{O}(\text{OH})}$



carbonyl group. This antibonding energy can be relieved by twisting the hydroxy group from the O-C=O molecular plane. This converts the antibonding C-O orbital into a non-overlapping molecular orbital which is nonbonding in character. Attempts to alleviate the antibonding density at the carbon and hydroxyl oxygen centres accompanying excitation, then accounts for the flexibility of formic acid in the  $S_1$  electronic state.

To conclude, from this study an understanding of the  $S_1$  state has emerged. Moreover, from this preliminary work, ideas concerning future experimental research can be proposed. By utilizing a laser system more powerful than the one used in these experiments, perhaps the supersonic jet and photoacoustic spectra of formic acid can be obtained with success. A complete analysis of the rovibrational band system is also essential: spectra at higher resolution would be valuable here. Of particular interest are the bands to the red of the origin. These bands, although not assigned in the present studies, do not appear to be due to hot bands which are related to the ground state vibrational frequencies. Could these bands be attributed to the syn species? To answer this question, temperature dependance studies are required. By increasing the temperature, the proportion of monomer to dimer will increase, thereby increasing the intensity of the vibrational system which should aid in the assignment of these





bands. Similarly, the bands to the blue in the spectrum appear to be somewhat featureless and have not been assigned. It is anticipated that these bands may be due to dimer; thus, an in depth analysis of this band system is required. Inevitably, these avenues of research will lead to interesting results as the spectroscopy of isomerisation and dimerisation in formic acid in the excited states are explored.



## REFERENCES

- (1) R. J. Gillespie, D. A. Humphreys, N. C. Baird, and E. A. Robinson, "Chemistry", Allyn and Bacon, Boston (1986).
- (2) T. Graedel, *Physics* 13, 345 (1987).
- (3) G. Winnewisser and E. Churchwell, *Astrophys. J.* 200, L33 (1975).
- (4) G. Herzberg and H. Verleger, *Z. Physik.* 37, 444 (1936).
- (5) S. H. Bauer and R. M. Badger, *J. Chem. Phys.* 5, 852 (1937).
- (6) L. Pauling and L. O. Brockway, *Proc. Natl. Acad. Sci.* 20, 336 (1934).
- (7) V. Z. Williams, *J. Chem. Phys.* 15, 232 (1947).
- (8) V. Z. Williams, *J. Chem. Phys.* 15, 243 (1947).
- (9) J. Karle and L. O. Brockway, *J. Amer. Chem. Soc.* 69, 2638 (1944).
- (10) V. Schomaker and J. M. O'Gorman, *J. Amer. Chem. Soc.* 69, 2638 (1947).
- (11) I. L. Karle and J. Karle, *J. Chem. Phys.* 22, 43 (1954).
- (12) R. G. Lerner, B. P. Dailey and J. P. Friend, *J. Chem. Phys.* 26, 680 (1957).
- (13) A. M. Mirri, *Nuovo Cim.* 18, 849 (1960).
- (14) G. H. Kwei and R. F. Curl, Jr., *J. Chem. Phys.* 32, 1592L (1960).
- (15) J. Bellet, A. Deldalle, C. Samson, G. Steenbbeckeliers and R. Wertheimer, *J. Mol. Structure* 9, 65 (1971).
- (16) A. Almennigen, O. Bastiansen and T. Motzfeldt, *Acta Chem. Scand.* 23, 2848 (1969).
- (17) T. Miyazawa and K. S. Pitzer, *J. Chem. Phys.* 30, 1076 (1959).
- (18) D. R. Lide, Jr., *Trans. Amer. Cryst. Assoc.* 2, 106 (1966).
- (19) I. C. Hisatsune and J. Heicklen, *Can. J. Spec.* 18, 135 (1973).
- (20) W. H. Hocking, *Z. Naturforsch* 31a, 1113 (1976).
- (21) E. Bjarnov and W. H. Hocking, *Z. Naturforsch* 33A, 610 (1978).
- (22) K. B. Wiberg and K. E. Laidig, *J. Am. Chem. Soc.* 109, 5935 (1987).
- (23) A. D. Clague and H. J. Bernstein, *Spectrochim. Acta* 2, 593 (1969).



- (24) Y. Chang, Y. Yamaguchi, W. H. Miller and H. F. Schaefer III, *J. Amer. Chem. Soc.* 109, 7245 (1987).
- (25) L. Pauling and L. O. Brockway, *Proc. Natl. Aca. Sci.* 24, 747 (1970).
- (26) R. C. Millikan and K. S. Pitzer, *J. Am. Chem. Soc.* 80, 3515 (1958).
- (27) G. L. Carlson, R. E. Witkowski and W. G. Fateley, *Spectrochim. Acta* 22, 1117 (1966).
- (28) D. Clague and A. Novak, *J. Mol. Struct.* 5, 149 (1970).
- (29) P. Excoffon and Y. Marechal, *Spectrochim. Acta Part A*, 28, 269 (1972).
- (30) J. Bournay and Y. Marechal, *Spectrochim. Acta Part A*, 31, 1351 (1975).
- (31) J. E. Bertie and K. H. Michaelian, *J. Chem. Phys.* 76, 886 (1982).
- (32) J. E. Bertie, K. H. Michaelian, H. H. Eysel and D. J. Hager, *H. Chem. Phys.* 85, 4779 (1986).
- (33) A. D. H. Clague and H. J. Bernstein, *Spectrochim. Acta. Part A* 25, 593 (1969).
- (34) H. Muller and H. J. Spangenberg, *Z. Chem.* 2, 91 (1962).
- (35) S. Tomoda and K. Kimura, *Bull. Chem. Soc. Jpn.* 56, 1768 (1983).
- (36) W. C. Price and W. M. Evans, *Proc. Roy. Soc. A* 162, 110 (1937).
- (37) S. Bell, T. L. Ng and A. D. Walsh, *J. Chem. Soc. Farad. Trans. II* 61, 393 (1974).
- (38) E. E. Barnes and W. T. Simpson, *J. Chem. Phys.* 39, 670 (1963).
- (39) S. Nagakura, K. Kaya and H. Tsubomura, *J. Mol. Spectrosc.* 13, 1 (1964).
- (40) C. Fridh, *J. Chem. Soc. Farad. Trans. II* 74, 190 (1978).
- (41) K. Kimura, S. Katsumata, T. Yamazaki and H. Wakabayashi, *J. Electron Spectrosc.* 6, 41 (1975).
- (42) C. R. Brundle, D. W. Turner, M. B. Robin and H. Basch, *Chem. Phys. Lett.* 3, 292 (1969).
- (43) D. Demoulin, *Chem. Phys.* 17, 471 (1976).
- (44) S. Iwata and K. Morokuma, *Theoret. Chim. Acta* 44, 323 (1977).
- (45) M. B. Robin, "Higher Excited States of Polyatomic Molecules", Volume II, Academic Press, New York (1975).



- (46) M. B. Robin, "Higher Excited States of Polyatomic Molecules", Volume III, Academic Press, Orlando (1985).
- (47) B. Sugarman, Proc. Phys. Soc. 55, 429 (1943).
- (48) T. L. Ng and S. Bell, J. Mol. Spectrosc. 50, 166 (1974).
- (49) K. Nishikawa and S. H. Lin, Chem. Phys. Lett. 149, 243 (1988).
- (50) T. Ebata, A. Fujii, T. Amano and M. Ito, J. Phys. Chem. 91, 6095 (1987).
- (51) M. Brouard and J. O'Mahony, Chem. Phys. Lett. 149, 45 (1988).
- (52) R. H. Judge and D. C. Moule, J. Mol. Spectrosc. 113, 302 (1985).
- (53) G. Fischer and Y. Sorek, J. Mol. Spectrosc. 74, 136 (1979).
- (54) G. Fischer, J. Mol. Spectrosc. 29, 37 (1969).
- (55) Gaussian 86, M. J. Frisch, J. S. Binkley, H. B. Schlegel, K. Raghavachar, C. F. Melius, R. L. Martin, J. J. P. Stewart, F. W. Bobrowicz, C. M. Rohlfing, L. R. Kahn, D. J. Defrees, R. Seeger, R. A. Whiteside, D. J. Fox, E. M. Fleuder, and J. A. Pople, Carnegie-Mellon Quantum Chemistry Publishing Unity, Pittsburgh PA, 1984.
- (56) M. Born and R. Oppenheimer, Ann. Physik 84, 457 (1927).
- (57) E. Schrodinger, Naturwissenschaften 14, 664 (1926).
- (58) W. H. Hehre, L. Radom, P. v.R. Schleyer and J. A. Pople, "Ab Initio Molecular Orbital Theory", John Wiley and Sons, New York (1986).
- (59) I. N. Levine, "Quantum Chemistry", 3rd Ed., Allyn and Bacon, Boston (1983).
- (60) T. Clark, "A Handbook of Computational Chemistry", John Wiley and Sons, New York (1985).
- (61) (a) C. C. J. Roothaan, Rev. Mod. Phys. 32, 179 (1960).  
(b) J. S. Binkley, J. A. Pople and P. A. Dobosh, Mol. Phys. 28, 1423 (1974).
- (62) J. A. Pople and R. K. Nesbet, J. Chem. Phys. 22, 571 (1954).
- (63) F. W. Bobrowicz and W. A. Goddard III, "Methods of Electronic Structure Theory", Chapter 4, Plenum Press, New York (1977).
- (64) W. A. Goddard III and L. B. Harding, Ann. Rev. Phys. Chem. 29, 363 (1978).





- (65) C. E. Dykstra, "Ab Initio Calculation of the Structures and Properties of Molecules", Elsevier Publishing Co., Amsterdam (1988).
- (66) C. Moller and M. S. Plesset, Phys. Rev. 46, 618 (1934).
- (67) (a) J. N. Murrell and A. J. Harget, "Semi-empirical Self-Consistent-Field Molecular Orbital Theory of Molecules", Wiley-Interscience, London (1971).  
 (b) J. A. Pople and D. L. Beveridge, "Approximate Molecular Orbital Theory", McGraw-Hill, New York (1970).
- (68) J. A. Pople, H. B. Schlegel, R. Krishnan, D. J. Defess, J. S. Binkley, M. J. Frisch, R. A. Whiteside, F. R. Hout, and W. J. Hehre, Int. J. Quantum Chem. 15S, 269 (1981).
- (69) G. W. King, "Spectroscopy and Molecular Structure", Holt, Rinehart and Winston Inc., New York (1964).
- (70) G. Herzberg, "Electronic Spectra of Polyatomic Molecules", D. Ban Nostrand Co. Inc., Princeton (1966).
- (71) W. A. Guillory, "Introduction to Molecular Structure and Spectroscopy", Allyn and Bacon Inc., Boston (1977).
- (72) G. Herzberg and E. Teller, Z. Physik. Chem. B21, 410 (1933).
- (73) J. A. Pople and J. W. Sjidman, J. Chem. Phys. 27, 1270 (1957).
- (74) E. U. Condon, Am. J. Phys. 24, 1104 (1956).
- (75) A. D. Walsh, J. Chem. Soc. 2306 (1953).
- (76) J. B. Coon, N. W. Naugle and R. D. McKenzie, J. Mol. Spectrosc. 20 107 (1966).
- (77) C. N. Barwell, "Fundamentals of Molecular Spectroscopy", McGraw-Hill Book Co. Ltd., London (1983).
- (78) J. E. Parkin, J. Mol. Spectrosc. 15, 483 (1965).
- (79) D. L. Andrews. "Lasers in Chemistry", Springer-Verlag, Berlin (1986).
- (80) M. L. Rutherford, D. J. Clouthier and F. J. Holler, Applied Spectroscopy 43, 532 (1989).
- (81) C. A. Hamer and J. P. Spoonhower, Applied Spectroscopy 38, 212 (1984).
- (82) G. R. Harrison, "M.I.T. Wavelength Tables", M.I.T. Press, Massachusetts (1969).
- (83) G. F. Kirkbright and S. L. Castleden, Chemistry in Britain 16, 661 (1980).



- (84) K. L. Kompa and J. Wanner, "Laser Applications in Chemistry", Plenum Press, New York (1984).
- (85) A. K. Skinner and D. W. Chandler, Am. J. Phys. 48, 8 (1980).
- (86) J. D. Graybeal, "Molecular Spectroscopy", McGrawHill Inc., New York (1988).
- (87) D. J. Clouthier and D. C. Moule, Topics in current Chemistry 150, 167 (1989).
- (88) J. C. D. Brand, J. H. Calloman and J. K. G. Watson, Disc. Far. Soc. 35, 175 (1963).















